Tectonophysics 653 (2015) 1–19

Contents lists available at ScienceDirect

Tectonophysics

journal homepage: www.elsevier.com/locate/tecto

Magnetotelluric array data analysis from north-west Fennoscandia

M. Cherevatova [a,*], M.Yu. Smirnov [a], A.G. Jones [b], L.B. Pedersen [c], MaSca Working Group
M. Becken [1] M. Biolik [2] M. Cherevatova [3] J. Ebbing [4] S. Gradmann [5] M. Gurk [2] J. Hübert [6] A.G. Jones [7]
A. Junge [8] J. Kamm [9] T. Korja [3] I. Lahti [10] A. Löwer [8] C. Nittinger [1] L.B. Pedersen [9] A. Savvaidis [11] M. Smirnov [3]

[1] The University of Münster, Germany
[2] University of Cologne, Germany
[3] University of Oulu, Finland
[4] Kiel University, Germany
[5] Geological Survey of Norway, Norway
[6] University of Alberta, Canada
[7] Dublin Institute for Advanced Studies, Dublin, Ireland
[8] University of Frankfurt, Germany
[9] Uppsala University, Sweden
[10] Geological Survey of Finland, Finland
[11] EPPO–Institute of Engineering Seismology and Earthquake Engineering, Greece

[a] University of Oulu, Finland
[b] Dublin Institute for Advanced Studies, Dublin, Ireland
[c] Department of Earth Sciences, Geophysics, Uppsala University, Uppsala, Sweden

ARTICLE INFO

Article history:
Received 16 July 2014
Received in revised form 4 December 2014
Accepted 13 December 2014
Available online 13 January 2015

Keywords:
Magnetotellurics
Fennoscandian Shield
2-D inversion
Lithosphere–asthenosphere boundary

ABSTRACT

New magnetotelluric (MT) data in north-west Fennoscandia were acquired within the framework of the project "Magnetotellurics in the Scandes" (MaSca). The project focuses on the investigation of the crustal and upper mantle lithospheric structure in the transition zone from stable Precambrian cratonic interior to passive continental margin beneath the Caledonian orogen and the Scandinavian Mountains in western Fennoscandia. An array of 59 synchronous long period and 220 broad-band MT sites was occupied in the summers of 2011 to 2013. We estimated MT transfer functions in the period range from 0.003 to 10^5 s.

The Q-function multi-site multi-frequency analysis and the phase tensor were used to estimate strike and dimensionality of MT data. Dimensionality and strike analyses indicate generally 2-D behaviour of the data with 3-D effects at some sites and period bands. In this paper we present 2-D inversion of the data, 3-D inversion models are shown in the parallel paper. We choose to invert the determinant of the impedance tensor to mitigate 3-D effects in the data on our 2-D models. Seven crustal-scale and four lithospheric-scale 2-D models are presented. The resistive regions are images of the Archaean and Proterozoic basement in the east and thin Caledonian nappes in the west. The middle and lower crust of the Svecofennian province is conductive. The southern end of the Kittilä Greenstone Belt is seen in the models as a strong upper to middle crustal conductor. In the Caledonides, the highly conductive alum shales are observed along the Caledonian Thrust Front. The thickest lithosphere is in the Palaeoproterozioc Svecofennian Domain, not in the Archaean. The thickness of the lithosphere is around 200 km in the north and 300 km in the south-west.

1. Introduction

The "Magnetotellurics in the Scandes" (MaSca) project targets development and application of the magnetotelluric (MT) method to study the Earth's structure in north-west Fennoscandia. The area of investigation consists of, from the oldest to the youngest formation, the Archaean Domain, the northern Svecofennian volcanic belt and the Caledonides. The array crosses two important boundaries: the ancient Archaean–Proterozoic boundary and the Caledonian Thrust Front (Fig. 1 a, b).

Prior to this project, there were no MT data acquired in western Fennoscandia, except for two recent MT profiles in southern Norway (Cherevatova et al., 2014) and across the central Scandinavian Mountains (Korja et al., 2008). A number of MT surveys have been conducted in the rest of Fennoscandia (Agustsson, 1986; Hjelt et al., 2006; Korja,

* Corresponding author.
E-mail address: maria.cherevatova@oulu.fi (M. Cherevatova).

http://dx.doi.org/10.1016/j.tecto.2014.12.023
0040-1951/

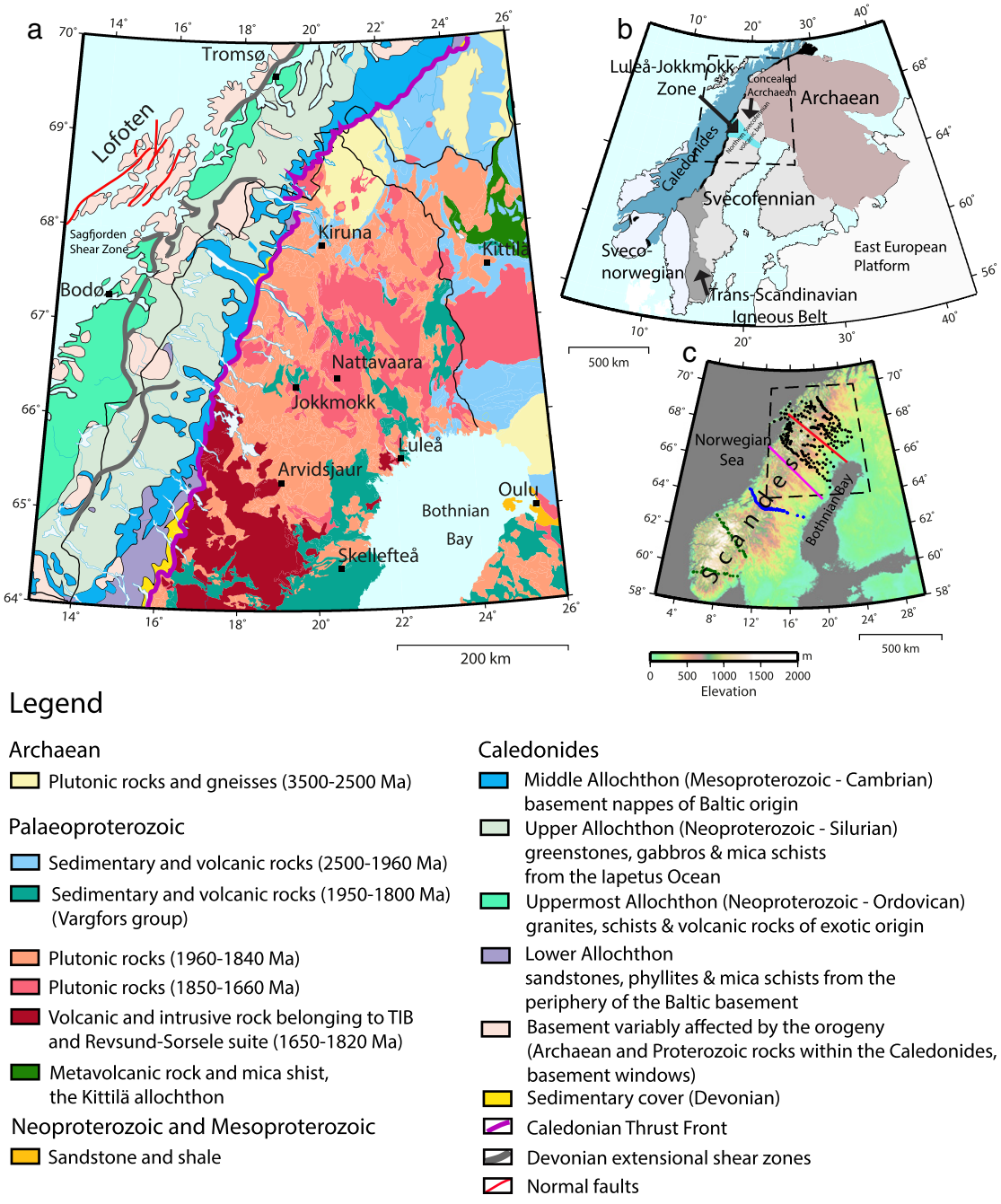

Legend

Archaean
- Plutonic rocks and gneisses (3500-2500 Ma)

Palaeoproterozoic
- Sedimentary and volcanic rocks (2500-1960 Ma)
- Sedimentary and volcanic rocks (1950-1800 Ma) (Vargfors group)
- Plutonic rocks (1960-1840 Ma)
- Plutonic rocks (1850-1660 Ma)
- Volcanic and intrusive rock belonging to TIB and Revsund-Sorsele suite (1650-1820 Ma)
- Metavolcanic rock and mica shist, the Kittilä allochthon

Neoproterozoic and Mesoproterozoic
- Sandstone and shale

Caledonides
- Middle Allochthon (Mesoproterozoic - Cambrian) basement nappes of Baltic origin
- Upper Allochthon (Neoproterozoic - Silurian) greenstones, gabbros & mica schists from the Iapetus Ocean
- Uppermost Allochthon (Neoproterozoic - Ordovican) granites, schists & volcanic rocks of exotic origin
- Lower Allochthon sandstones, phyllites & mica schists from the periphery of the Baltic basement
- Basement variably affected by the orogeny (Archaean and Proterozoic rocks within the Caledonides, basement windows)
- Sedimentary cover (Devonian)
- Caledonian Thrust Front
- Devonian extensional shear zones
- Normal faults

Fig. 1. Main geological units of the Caledonian orogen and the Precambrian basement in north-west Fennoscandia. (a) Simplified geology map. The map is compiled after Gorbatschev and Bogdanova (1993), Ramberg et al. (2008) and Ebbing et al. (2012). (b) Main tectonic domains in Fennoscandia (modified from Koistinen et al. (2001)). (c) Elevation map: black circles — MaSca array, blue — Jämtland–Trøndelag magnetotelluric profile (Korja et al., 2008), green — ToSca MT profiles (Cherevatova et al., 2014), red line — seismic SCANLIPS experiment (Ebbing et al., 2012), magenta line — the Blue Road seismic profile (Lund, 1979).

2007; Korja et al., 1989; Korja et al., 2008; Lahti et al., 2005; Rasmussen, 1988; Rasmussen et al., 1987) and its margins (Brasse et al., 2006; Jones, 1983; Smirnov and Pedersen, 2009). The Baltic Electromagnetic Array Research (BEAR) project was an international experiment for deep electromagnetic sounding. Earlier studies together with the BEAR data allowed compilation of a map of integrated conductance of the Fennoscandian Shield and its margins (Korja et al., 2002). Accordingly, the MaSca project is a natural continuation of MT measurements to the north-west.

Seismic and electromagnetic methods are two geophysical techniques that can measure the in situ physical properties of the lithosphere. Knowledge of the geometry of the lithosphere–asthenosphere boundary (LAB) is important as this boundary significantly controls the geodynamic processes that create, modify, and destroy the lithosphere. The MaSca array is aimed at measurements of the electric properties to give a new insight into the thickness of the lithosphere.

Unfortunately, north-west Fennoscandia is not well studied by seismic methods. Therefore, a comparison of the resistivity and velocity models is not currently possible. In Sweden, the European Geotraverse and related experiments provide information on the central part of the Fennoscandian Shield (Guggisberg et al., 1991; Lund and Heikkinen, 1987). The results of these show a thickened crust below the low topography of the central Fennoscandian Shield, which is not in agreement with the observed gravity signal. The Blue Road profile across the

northern Scandinavian Mountains (Lund, 1979) is located some 100 km to the south from MaSca array. Lund (1979) stated that there is evidence for a shear (S) wave low-velocity zone of a few tens of kilometres in the uppermost mantle.

This paper is focused on 2-D inversion of MaSca data. In the current study we perform detailed strike and dimensionality analyses using Q-function multi-site and multi-frequency approach of Zhang et al. (1987) and the phase tensor approach of Caldwell et al. (2004). Theoretically, both techniques are expected to give the same estimates of the strike direction and dimensionality; however, in the presence of noise and strong distortion they may have differing resolution and estimation properties (see e.g., Jones (2012)). Thus, a comparative analysis is shown for MaSca measurements. Since the data exhibit some 3-D behaviour, 2-D inversion models are obtained by inverting the determinant of the impedance tensor. The determinant has certain advantages compared to bi-modal inversion in cases where data show 3-D effects (Pedersen and Engels, 2005). Inversions were separated into crustal- and lithospheric-scale. To resolve the crustal features we selected 7 profiles Crust 1–7 and 4 profiles Lithos 1–4 to resolve the thickness of the lithosphere (Fig. 2).

2. Geological background

The crust beneath the MaSca array consists of three distinct units viz. the Archaean Domain (3.1–2.9 Ga Saamian orogeny, Lopian orogeny 2.9–2.6 Ga) in the north-east, the Svecofennian Domain (2.0–1.75 Ga) in the east, and Caledonian orogen (0.6–0.4 Ga) in the west (Gaál and Gorbatschev, 1987) (Fig. 1b).

The Archaean Domain is a typical Neoarchaean granitoid-greenstone province comprising granitoid gneiss complexes and supracrustal rocks ranging in age between 3.1 and 2.6 Ga. The Archaean rocks are overlain by Palaeoproterozoic cover rocks deposited on Archaean basement since 2.45 Ga (Central Lapland Schist Belt). In the north-western part of the Archaean Domain (northern Finland and Sweden), large areas are intruded by 1.9–1.8 Ga old plutonic rocks (Central Lapland Granitoid Area) (Korja et al., 2002).

The Scandinavian Caledonides (Fig. 1) were formed as the result of a closure of the Iapetus Ocean and continental collision of Baltica and Laurentia in the Late Silurian (Gee et al., 2008; Gorbatschev and Bogdanova, 1993; Ramberg et al., 2008; Roberts, 2003; Rykkelid and Andresen, 1994). During the Caledonian orogeny (540–400 Ma), Precambrian rocks on the western margin of Baltica were thrust beneath Laurentia to ultra-high pressure depths. The underthrust rocks of Baltica were heated, metamorphosed and deformed (Andersen, 1998), whereas rocks of the Neoproterozoic to Early Palaeozoic accretionary wedge were transported to the east/north-east over Baltica as Caledonian nappes. The Caledonian mountains were eroded during the Devonian. The extensional collapse of the Scandinavian Caledonides resulted in rapid tectonic denudation of the orogen, exhumation of high- to ultra-high-pressure metamorphic rocks and provided a structural template for the formation of Devonian supra-detachment sedimentary basin (Andersen, 1998). The extensional shear zones and fabrics indicate W- to NW-directed translations (Gee et al., 2008).

The Archaean Domain and most of the Svecofennian Domain have crustal thickness of 40–50 km. The region of the anomalously thick crust in the Fennoscandian Shield is located at the Archaean–Proterozoic suture zone (Korja, 1993). In the Caledonides, crustal thickness is 32 km at the Norwegian coast and increases to 43 km beneath the central Scandinavian Mountains (Ebbing et al., 2012).

Magnetotellurics rarely images the base of the crust (e.g. (Jones, 2013)). The best resolved parameter in MT is the top of a conducting layer. Therefore, for long period MT data the top of the asthenosphere (or base of the lithosphere) can be detected with high-quality data regardless of the primary cause of enhanced conductivity in asthenosphere (H+ or a small fraction of partial melt). As a consequence, the MT method is well suited to map the depth to lithosphere–asthenosphere boundary (LAB) (Jones, 1999). According to Korja (2007), the "thickest" lithosphere is in the Palaeoproterozoic Svecofennian Domain (300 km) not in the Archaean; lithosphere is thinning towards the Atlantic and Arctic Oceans as well as to the east (100 km).

3. Data acquisition and processing

The MaSca array covers 350 km by 480 km area and stretches from Tromsø and Bodø (Norway) in the west to Kiruna and Skellefteå (Sweden) in the east (Fig. 1). The project commenced in the summer of 2011 and data collection continued until summer 2013, resulting all together in 59 synchronous long period (LMT) and 220 broad-band (BBMT) sites. The average separation between LMT sites is 30 km, and 10 km between BBMT; however there are gaps of 50–80 km in places

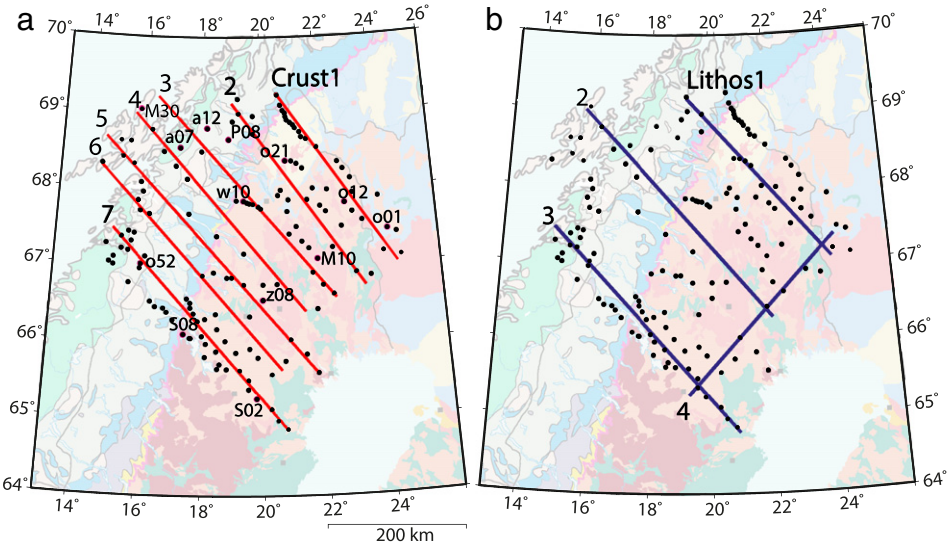

Fig. 2. Location of the magnetotelluric stations plotted on top of the geological map (Fig. 1). (a) Crustal-scale 2-D inversion profiles: Crust 1–7. (b) Lithospheric-scale 2-D inversion profiles: Lithos 1–4.

because of inaccessibility due to the high topography in the region of the Scandinavian Mountains. We also used other available data sets from the MaSca area. These are six MT sites from BEAR array (Lahti et al., 2005; Varentsov et al., 2002), four vertical component measurements from the IMAGE observatories (http://space.fmi.fi/image/), and two small arrays of Finnish Geological Survey (GTK) (Lahti et al., 2012).

Broad-band MT data were collected in the frequency range from 0.001 to 300 Hz with the MTU2000 MT system developed at Uppsala University, Sweden (Smirnov et al., 2008). The duration of recordings was usually one day (i.e., around 20 h). Broad-band MT data were continuously sampled at 20 Hz and simultaneous burst recordings with 1000 Hz sampling were recorded for 2 h starting at midnight. During the field campaigns, we did not measure the vertical magnetic field H_z at every site. All LMT sites were occupied for about two months. The same MTU2000 system together with LEMI120 instruments was used to acquire LMT data. All the transfer functions were estimated using multi-remote reference technique (Smirnov, 2003) as well as novel multivariate analysis technique (Smirnov and Egbert, 2012), thus providing stable transfer function in the period range from 0.003 to 10^5 s at BBMT + LMT sites and 0.003–1024 s at BBMT only sites. The array is located at high geomagnetic latitudes therefore application of multivariate technique was vital to validate source field free transfer functions.

Data examples are shown in Fig. 3 for selected sites from different areas. Sites o21 and S08 are examples of high resistivity curves; P08 — low resistivity; P08 and o12 are examples of phases out of quadrant; M10, M30 and S08 — long curves, up to 10^5 s. In general apparent resistivity shows varying behaviour along the profiles, indicating the complexity of the geoelectrical structure of the area. At some sites the highest value is over 10^5 Ωm whereas at some others it is lower than 0.1 Ωm depending on the underlying geological units.

We have used the following criteria to evaluate data quality and perform data selection. First, we discarded highly scattered impedance estimates having large error bars. We also checked that impedance tensor

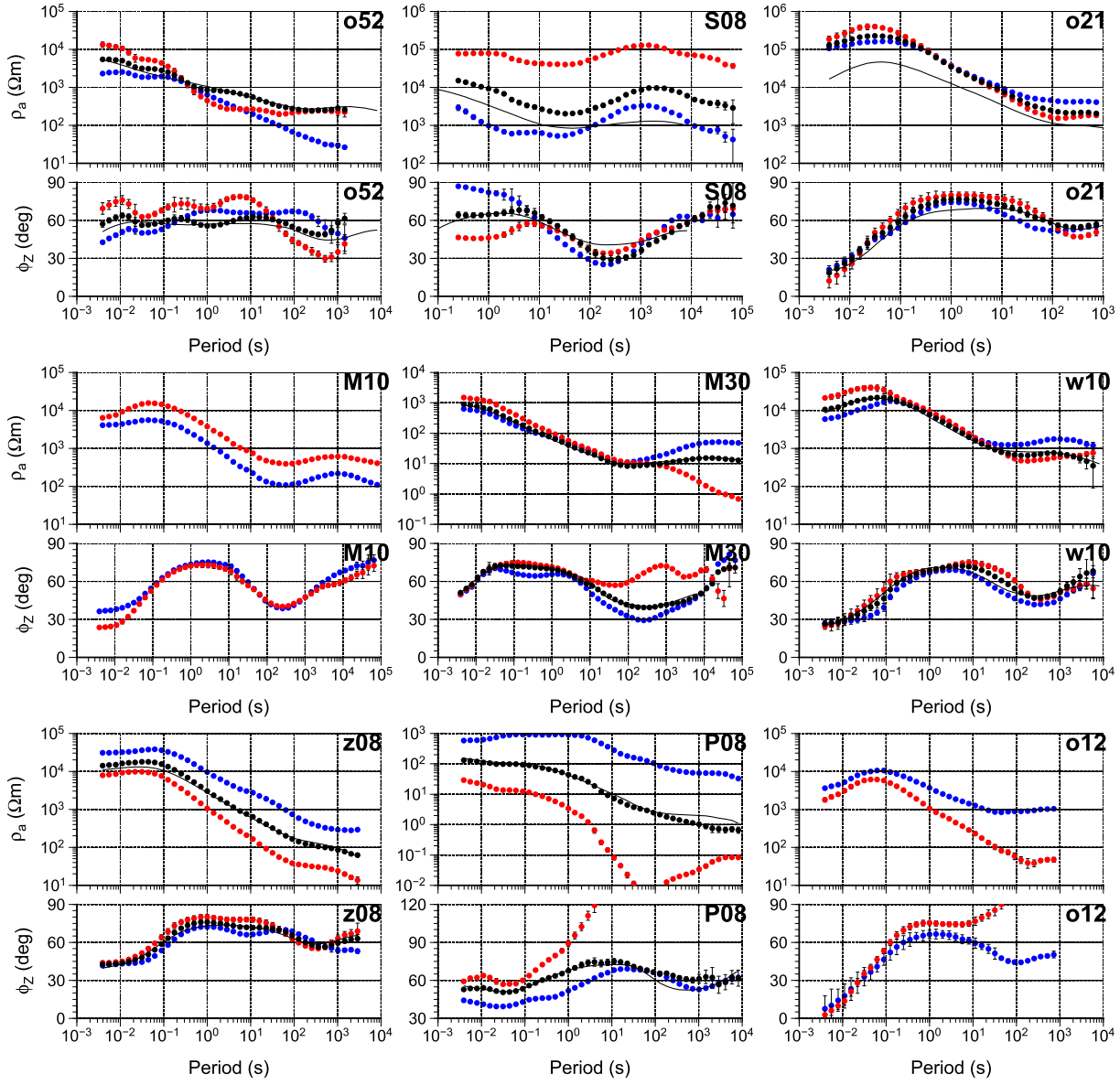

Fig. 3. Examples of the observed apparent resistivity and phase from MaSca array. Blue circles — Z_{xy}; red — Z_{yx}; black — Z_{det}; solid black curves represent 2-D model responses for Z_{det} data (Fig. 10); vertical bars give confidence limits (95%). Sites o21 and S08 are examples of high resistivity curves; P08 — low resistivity; P08 and o12 are examples of phases out of quadrant; M10, M30 and S08 — long curves, up to 10^5 s (see Fig. 2 for locations of the sites).

parameters, like skew values, phase tensor and strike are stable, varying smoothly with period. Secondly, apparent resistivity and phase should be consistent in order to satisfy dispersion relations which are proven to be valid for 1-D and 2-D TM-mode models (Berdichevsky and Pokhotelov, 1997; Weidelt and Kaikkonen, 1994). We used this relation as the last criterion for data selection.

4. Strike and dimensionality analysis

4.1. Q-function analysis

The internal structure of the impedance tensor allows us to derive all necessary information about the dimensionality and strike (if 2-D or quasi 2-D) of the underlying medium. We conduct strike and dimensionality analysis to assess to what extent the data can be interpreted in a 2-D sense on a regional scale and to define the appropriate profile direction. A standard model of a 2-D regional structure perturbed by 3-D small-scale subsurface inhomogeneities is considered. Following the approach of Zhang et al. (1987) makes it possible to estimate the strike direction based on multi-site and multi-frequency averaging. Details of the practical use of the method (Q-function analysis) can be found in Smirnov and Pedersen (2009).

According to approach of Zhang et al. (1987), the distorted impedance tensor (Z) is expressed in terms of undistorted impedance tensor (Z^r) as

$$Z \approx (I + P_h) Z^r, \tag{1}$$

where I is the identity matrix and P_h is the distortion matrix. Note, that the magnetic field is relatively free of galvanic distortion caused by local structures, whereas the electric field will be distorted as described by the real distortion tensor (P_h). In the case of the decomposition model, 2-D regional structure and 3-D local structure, in the coordinate system aligned with the strike

$$Z = \begin{bmatrix} P_{xy} Z^r_{yx} & (1 + P_{xx}) Z^r_{xy} \\ (1 + P_{yy}) Z^r_{yx} & P_{yx} Z^r_{xy} \end{bmatrix}. \tag{2}$$

Thus the column elements are related by real constants ζ and γ

$$Z = \begin{bmatrix} \zeta Z^r_{yx} & Z^r_{xy} \\ Z^r_{yx} & \gamma Z^r_{xy} \end{bmatrix}, \tag{3}$$

where

$$\zeta = \frac{P_{xy}}{(1 + P_{yy})}, \quad \gamma = \frac{P_{yx}}{(1 + P_{xx})} \tag{4}$$

and the diagonal components of the impedance tensor are related to the off-diagonal impedance elements in the same column as:

$$\begin{matrix} Z_{xx} = \zeta Z_{yx} \\ Z_{yy} = \gamma Z_{xy} \end{matrix}. \tag{5}$$

Note that ζ and γ can be expressed in terms of twist and shear parameters (β and γ) of Groom and Bailey (1989) (Eq. (23)) and do not include gain factors of electric field. Estimates ζ, γ and strike angle are thus determined by minimizing the target functional

$$Q = \frac{1}{4N - 3N_p - 1} \times \sum_i \sum_j \left(\frac{1}{\sigma^2_{yx_{ij}}} \left| Z_{xx_{ij}} - \zeta_i Z_{yx_{ij}} \right|^2 + \frac{1}{\sigma^2_{xy_{ij}}} \left| Z_{yy_{ij}} - \gamma_i Z_{xy_{ij}} \right|^2 \right), \tag{6}$$

where the indexes i and j refer to stations and periods over which the averaging is done, $N = N_p N_s$ with N_p denoting the number of periods and N_s the number of stations. Therefore, the strike direction is defined by searching for the minimum of the Q-functional. For a fixed strike, $\sqrt{Q}$ is used as a measure of whether the data support the assumption of a 2-D regional structure underlying a local 3-D distorter. The impedance elements are also weighted by errors (σ_{xy} or σ_{yx} in Eq. (6)), we used the fixed error floor of 5% of the corresponding off-diagonal impedance elements because the estimated errors are generally too small (Smirnov and Pedersen, 2009). For these conditions, the expectation value of $\sqrt{Q}$ will be unity. The stable strike direction for all sites and periods and small $\sqrt{Q}$-function estimates are necessary condition of data to be described by 2-D regional model.

Maps of Q-function rose diagrams are presented in Fig. 4 (right panels) for periods that range from 1 to 100 s (top) and from 100 to 10^4 s (bottom). The rose diagrams are plotted for groups of sites, using averaging by sites and one or two decades by periods. A few dominant strike directions can be observed. At the shorter periods of 1–100 s: (i) in the south-west the strike is N60°E–N70°E and rotates to N80°E–N90°E northward; and (ii) in the east, almost all rose diagrams show NS striking structure. At the longer periods of 100–10^4 s: (i) in the west two strikes can be observed: N30°E and NS, (ii) in the east, most of rose diagrams rotated to N40°E–N50°E, however there is evidence of NS directions.

For determination of geoelectric strike, there is an ambiguity of 90° in strike estimation from Q-functions, thus additional information from induction vectors is required. In Fig. 4 (left panels), maps of the real induction vectors (Wiese convention) are presented for periods of 32 s and 1024 s. When the structure is 2-D all these vectors are parallel and point away from electric current concentrations (Booker, 2012). The vectors are thus perpendicular to 2-D strike. At a period of 32 s, the induction vectors point in different directions, identifying 3-D small scale near-surface structures. Along the western margin, induction vectors point away from the Atlantic Ocean and in the south-east they identify a highly conductive anomaly in the south of the Skellefteå district. At a period of 1024 s, the vectors are more co-linear showing 2-D regional structure. The amplitude of the vectors increases, implying highly conductive structures: the Atlantic Ocean and the Skellefteå conductor, characterized by 4000 S crustal conductance (Korja, 2007). To the east of the Caledonian Thrust Front, the induction vectors are north-east directed. This is possibly due to superposition of both the ocean and Skellefteå effects. The array is located at high latitudes, therefore the source field can especially affect the induction vectors (Jones and Spratt, 2002; Smirnov and Egbert, 2012). At longer periods (>5800 s), the source field effect is revealed through the rotating of the induction vectors to the north. This issue requires further investigation and is not a topic of the present study.

To summarize, on average the central regional structure is characterized by N45°E strike from the Q-function rose diagrams. It also agrees with the structural data, having a dominant geological strike in a NNE–SSW direction in the west, but contradicts to strike N45°W for geological mapping in the east. The tipper data are doubtful with regard to strike direction, as they are affected by the coast effect. Therefore, they cannot be used as supporting information for strike determination. Since there is no preferable strike direction for all periods and sites, we choose to invert the determinant of the impedance tensor, which is invariant under rotation. The selected azimuth of the profiles is N135°E, however we also present the model for azimuth N45°E in the east.

4.2. The magnetotelluric phase tensor

The phase tensor geometry provides information about directionality and dimensionality of regional conductivity structure. This information is

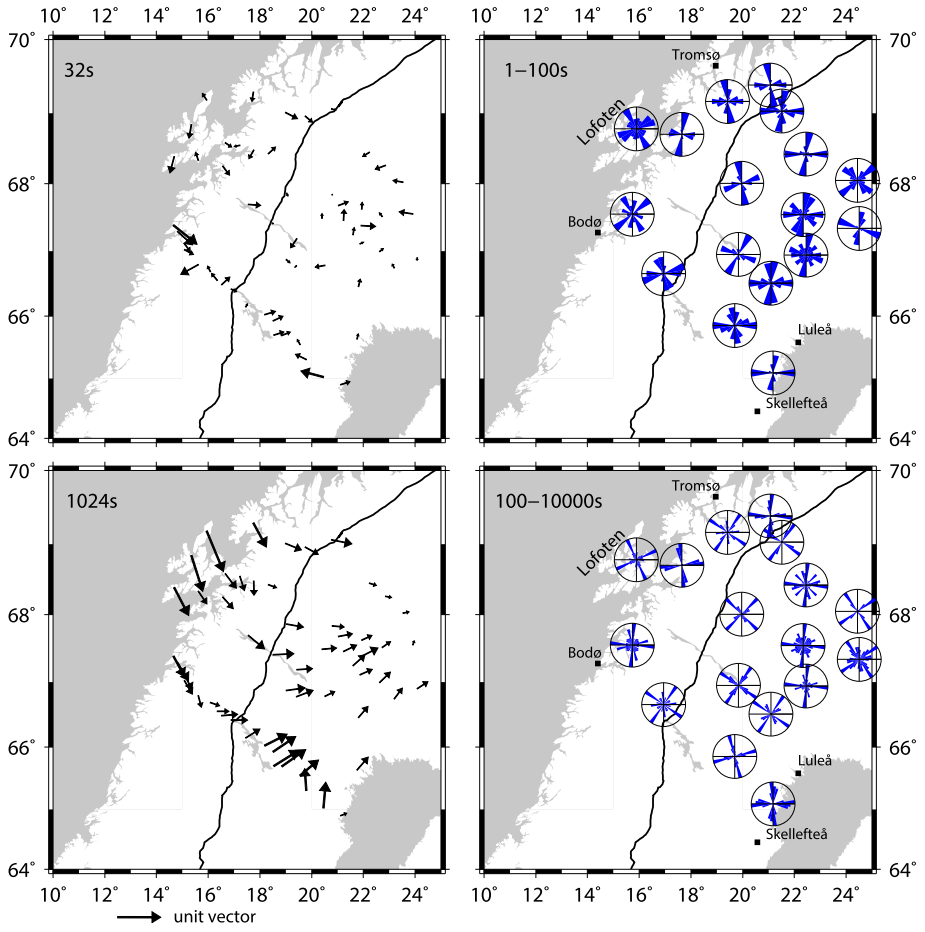

Fig. 4. Strike and dimensionality analysis. Left panels — real Wiese induction vector map for periods 32 s and 1024 s. Right panels — Q-function rose diagrams for periods 1–100 s and 100–10^4 s. Black thick line — Caledonian Thrust Front.

widely used to justify 2-D interpretation (Booker, 2012). The MT phase tensor defined by the relation

$$\Phi = X^{-1}Y = \begin{pmatrix} \Phi_{xx} & \Phi_{xy} \\ \Phi_{yx} & \Phi_{yy} \end{pmatrix}, \tag{7}$$

where **X** and **Y** are real and imaginary parts of the complex impedance tensor **Z** and Φ is real. The phase tensor has the following properties: (i) the phase tensor is unaffected by the frequency independent electric effects of galvanic distortion, (ii) its skew is zero when the regional structure is 2-D, and (iii) it gives the information about the direction of the regional structure. The phase tensor can be depicted graphically as an ellipse, with the major and minor axes of the ellipse representing the principle axes of the tensor (Caldwell et al., 2004). The orientation of the major axis is specified by the skew angle (β) and angle (α) that expresses the tensor's dependence on the coordinate system:

$$\Phi = R^T(\alpha-\beta)\begin{bmatrix} \Phi_{max} & 0 \\ 0 & \Phi_{min} \end{bmatrix} R(\alpha+\beta), \tag{8}$$

where Φ_{max} and Φ_{min} are the lengths of ellipse semi-axes and the skew angle

$$\beta = \frac{1}{2} arctan\left(\frac{\Phi_{xy}-\Phi_{yx}}{\Phi_{xx}+\Phi_{yy}}\right). \tag{9}$$

and

$$\alpha = \frac{1}{2} arctan\left(\frac{\Phi_{xy}+\Phi_{yx}}{\Phi_{xx}-\Phi_{yy}}\right). \tag{10}$$

The angle $\theta = \alpha - \beta$ is the strike or its perpendicular. The skew angle estimate has also corresponding errors which need to be taken into account when analysing dimensionality. There are two simple ways to estimate skew errors, i.e. using error propagation or delta method and parametric bootstrap. The latter is easy to implement, however it requires to make assumptions about distribution and covariance. We assumed that all components of impedance tensor are uncorrelated having Gaussian distribution. We generated 1000 bootstrap replicants and consequently estimated mean square error. Similarly to Q-function estimates we used the fixed value of 5% of the corresponding off-diagonal impedance elements (σ_β) instead of real errors. After that, we considered the skew angle with subtracted standard errors: $\beta_{res} = |\beta| - \sigma_\beta$, where

$$\tilde{\beta} = \begin{bmatrix} \beta_{res}, & \beta_{res} > 0 \\ 0, & \beta_{res} < 0 \end{bmatrix}. \tag{11}$$

It means that we only have taken into account significant part of skew values exceeding error estimate. Here we used 95% confidence limit. In the following discussion we use the residual of the skew angles $\tilde{\beta}$, applying the recommendation of Booker (2012) that the skew angle is zero when the structure is 2-D and less than 3° for structure to be

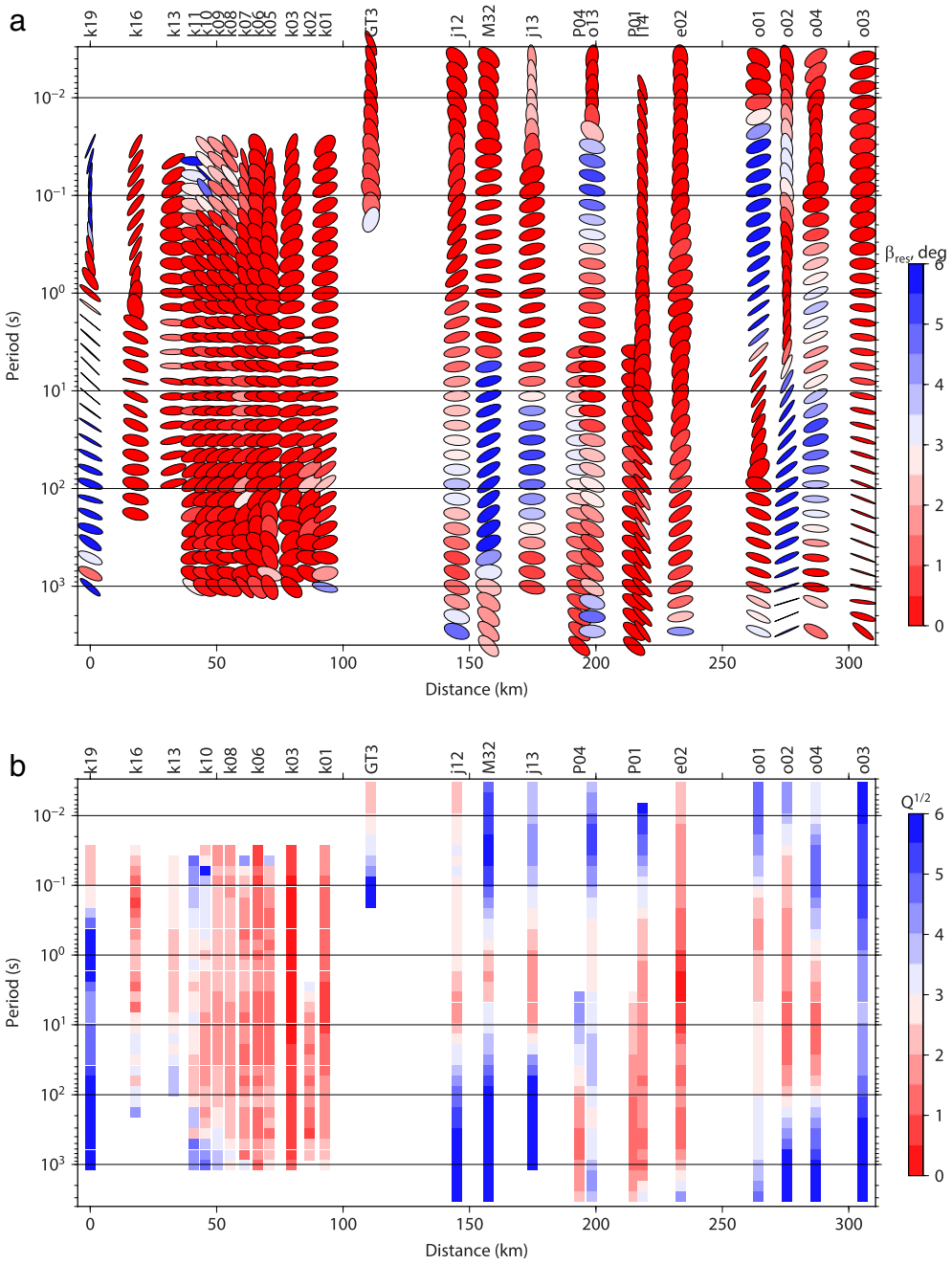

Fig. 5. Strike and dimensionality analysis for profile Crust 1 (Fig. 2). Comparison of the phase tensor ellipses and Q-function estimates. (a) Phase tensor ellipses with the skew angle colour fill. The colour scale uses residuals of $\tilde{\beta}$, Eq.(11). Red colours are considered to be quasi-2-D, blue — significant 3-D effects. (b) $\sqrt{Q}$-function estimate for all sites and periods along the profile for N45°E strike direction. Red colours are considered to be quasi-2-D within 15% error on the impedance tensor, blue — significant 3-D effects, or deviation from the strike.

quasi-2-D (2-D hereafter). However, small skew value at a single period is not a sufficient condition for a 2-D assumption, it is also necessary that it remains sufficiently small at all periods. Furthermore, it is necessary that θ be constant as a function of period and along the profile or throughout an array (Booker, 2012). The inconsistent variation in the direction of the axis of the tensor ellipse is an indicator of 3-D situation, even if the $\tilde{\beta}$ values are small (Caldwell et al., 2004).

In Figs. 5 and 8, we present the phase tensor ellipses, plotted for two 2-D inversion profiles Crust 1 and 7 (see locations in Fig. 2). Pseudo-sections of $\sqrt{Q}$-function estimates are presented for a comparison of the two approaches. The phase tensor ellipses with skew angle $\tilde{\beta}$ (Eq. (11)) as the colour fill are shown in Fig. 5a for all sites along Crust 1 profile and by periods. Red colours in Fig. 5a are considered to be 2-D.

The phase tensor ellipses show consistent patterns throughout the period range and along the profile, indicating good data quality. The phase tensor skew values and $\sqrt{Q}$-function estimates are mostly less than 3°, however there are certain regions with high skew. Thus, the deviation of the impedance tensor from the 2-D assumption is estimated to be at the level of 15% for $\sqrt{Q}$-function of 3 with the 5% error floor. A region of low skew can be seen to lie between sites k01 and k13 for the entire period range. The values of $\sqrt{Q}$-function are less than 10% of 2-D. In the east, the phase tensor skew and $\sqrt{Q}$-function estimates are also consistent, except for an area at short periods and site o03. In

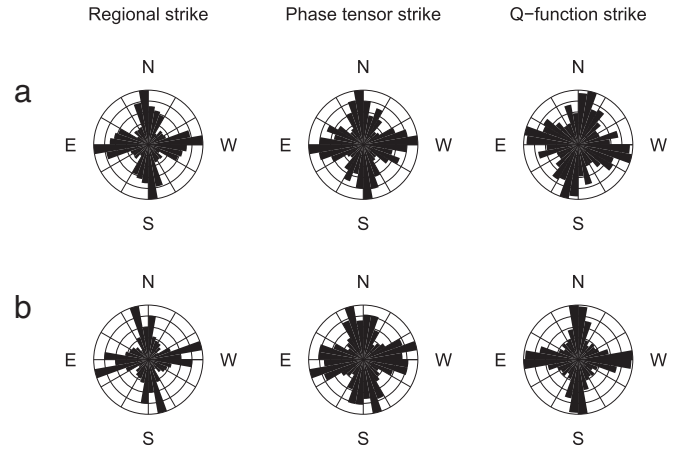

Fig. 6. Cumulative rose diagrams of the regional strike according to Bahr (1991), the phase tensor strike (Caldwell et al., 2004) and Q-function strike (Zhang et al., 1987) for Crust 1 (a) and Crust 7 (b) profiles. The period range is 1–1000 s, the resolution of the rose diagrams is 10°.

this region, the phase tensor ellipses exhibit 2-D behaviour, $\widetilde{\beta}<2$, but $\sqrt{Q}$-function more than 15%, thought to be 3-D. $\sqrt{Q}$-function is computed for the selected strike direction. It shows high estimates in two cases, when the structure is 3-D and if the strike angle is incorrect. From the plots of the phase tensor ellipses we can see that strike in this region is 0° and strike used for $\sqrt{Q}$-function calculations is 45°. Therefore the inconsistent behaviour of $\sqrt{Q}$-function is due to different strike directions. Overall, the phase tensor and $\sqrt{Q}$-function skews are consistent, showing 2-D regional structure within 15% error of the impedance tensor.

Fig. 6a shows rose diagrams of the strike direction determined from Bahr's (Bahr, 1991) regional strike, the phase tensor and Q-function for profile Crust 1. The diagrams are plotted for the period range of 1–1000 s and three sites and one decade in period were used for Q-function computation. Both regional and phase tensor diagrams define NS dominant strike direction, but there is evidence of the second strike of N30°E in the phase tensor plot. The Q-function rose diagrams show the main strike rotated by 10° east of north. There are also indications of N30°E and N70°E striking structures.

In Fig. 7 the phase tensor ellipses are shown together with the real induction vectors in Wiese convention. Induction vector information is not always comparable with the phase tensor, because they do not sample the same volume. The induction vectors and major axes of the phase tensor are parallel (or perpendicular) for most sites and periods. The magnitude of the induction vectors increases with period and they rotate to NNE, indicating a coast effect. The same behaviour is observed at other profiles (not shown). At shorter periods (less than 1000 s) the induction vectors are small, inferring that there is no induction effect caused by large lateral contrasts in conductivity. At longer periods the source field affects the induction vectors by rotating them to the north, for example at sites P03, MUO, P04, P01 and M22.

In Fig. 8a the phase tensor ellipses for the south-western profile Crust 7 are presented (see Fig. 2 for location). Contrary to Crust 1, these data contain more apparent 3-D effects. In the west, the phase tensor ellipses are narrow and the direction of the major axes changes sufficiently. Together with the high skew values, of more than 3°, this is clear indication of 3-D regional structure(s). The $\sqrt{Q}$-function skew is 4 (20%) and is higher in the north-western compared to the south-eastern ends of the profile (Fig. 8b). To the south-east, some indications of 2-D structure appear, such as skew is generally lower and ellipses are more rounded. There is a discrepancy between $\sqrt{Q}$-function and the phase tensor ellipses in the east. Particularly, at shorter periods, less than 0.1 s, the phase tensor skew is around 2°, but $\sqrt{Q}$-function estimate is higher: 3 to 4. This inconsistency may be due to averaging by periods, used to calculate $\sqrt{Q}$-function or by the incorrect strike (see discussion above for the Crust 1 case), or by the manner in which the estimates are derived.

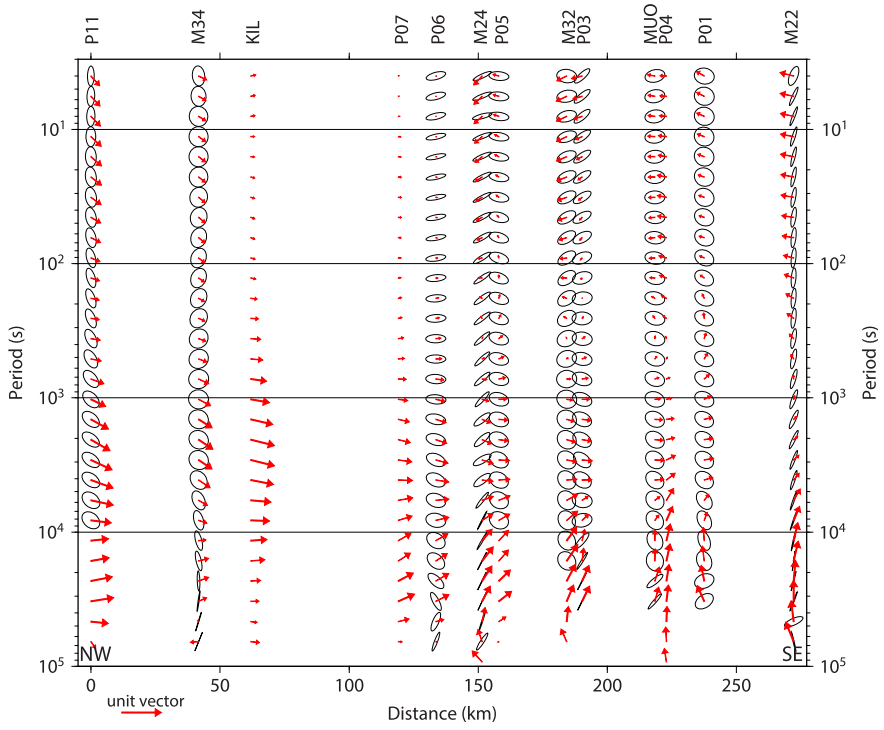

Fig. 7. Scaled phase tensor ellipses with real Wiese induction vectors at 13 sites along profile Crust 1 (Fig. 2).

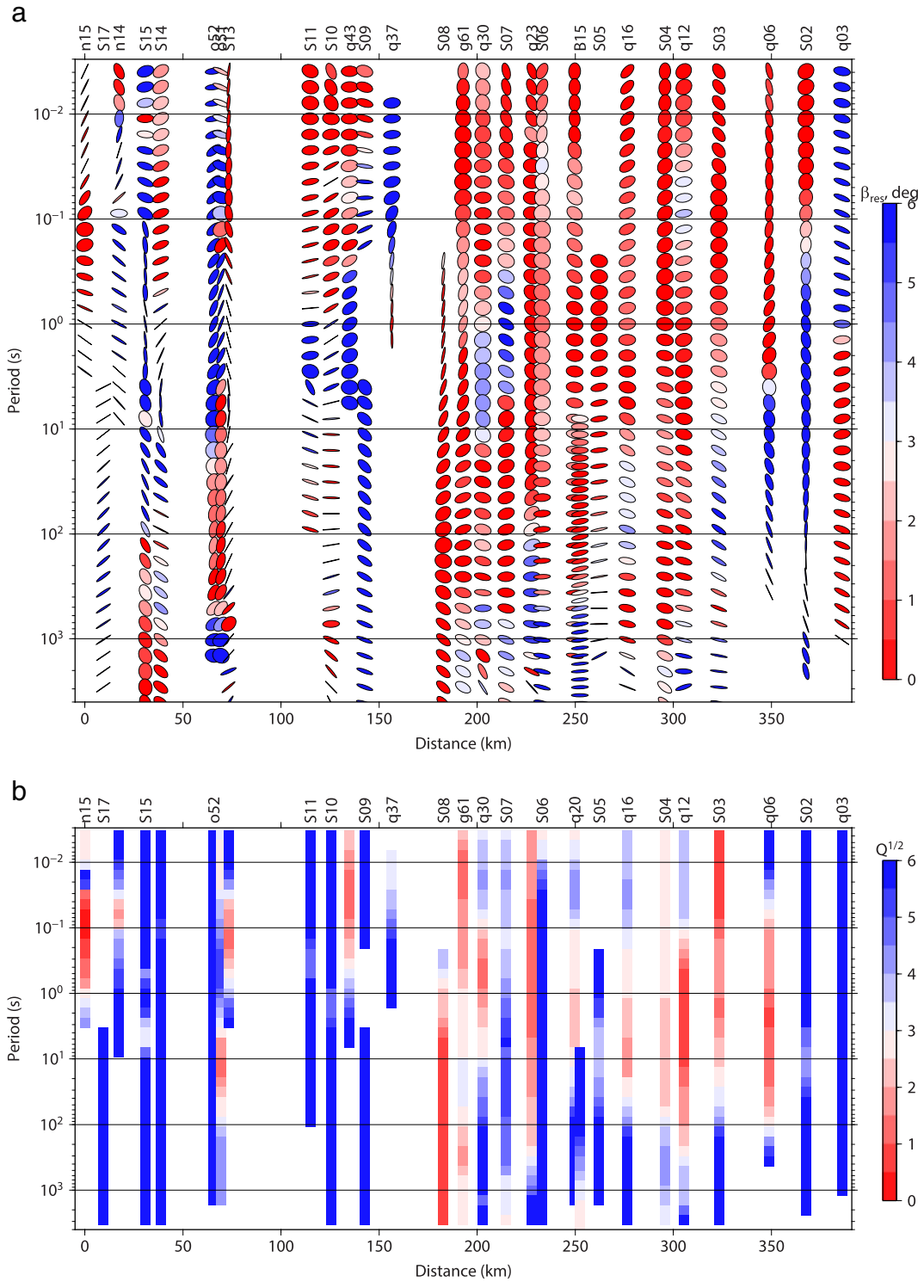

Fig. 8. Strike and dimensionality analysis for profile Crust 7 (Fig. 2). Comparison of the phase tensor ellipses and Q-function estimates. (a) Phase tensor ellipses with the skew angle colour fill. The colour scale uses residuals of $\widetilde{\beta}$, Eq. (11). Red colours are considered to be quasi-2-D, blue — significant 3-D effects. (b) $\sqrt{Q}$-function estimate for all sites and periods along the profile for N45°E strike direction. Red colours are considered to be quasi-2-D within 15% error on the impedance tensor, blue — significant 3-D effects, or deviation from the strike.

The cumulative rose diagram for the strike estimated by Bahr's method (Fig. 6b) shows the main N80°E and N10°E additional directions. This is supported by the phase tensor diagram, which is more scattered describing more variations in the strike. The Q-function rose diagram is NS directed and represents the average between two strikes, shown in other methods.

To conclude, the Q-function and the phase tensor analyses generally give the same estimates of the dimensionality and strike direction of the structure. However, some discrepancies are apparent, probably related to averaging over periods/sites applied for Q-function. The advantage of the Q-function is that it gives a quantitative estimate of the deviation of the impedance from 2-D assumption. The same analyses have been

done for all data (all 2-D profiles) and the general conclusions are valid for them.

The phase tensor ellipses at a period of 16 s are shown in Fig. 9. To the west of the Caledonian Thrust Front the phase tensor ellipses reflect 3-D regional structure(s). Near the fault zones, the narrow ellipses rotate significantly responding to the complicated 3-D nature of the Caledonian nappes. Similar pattern has been observed in Q-function rose diagrams at periods 1–100 s (see above). To the east of the Caledonian Thrust Front, the ellipses show 2-D structure. Some areas are characterized by the skew angle of less than 3°, for example in the north-east. The northernmost dense "K sites" cross the Caledonian Thrust Front. The phase tensor ellipses are changing from the clear 3-D behaviour in the west to 2-D towards east.

5. 2-D inversion

In this section we present 2-D inversion models, obtained by inverting the determinant of the impedance tensor. Inversions were separated into crustal- and lithospheric-scale. To resolve the crustal features, we selected 7 profiles Crust 1–7 and 4 profiles Lithos 1–4 to resolve the thickness of the lithosphere (Fig. 2). According to the strike analysis (Section 4) an average strike of N45°E can be selected, consequently the azimuth of the profiles is N135°E. Different inversion algorithms were implemented, such as Occam (Constable et al., 1987), Rebocc (Siripunvaraporn and Egbert, 2000) and smoothed damped least squares (Cherevatova et al., 2014). In this study, we present the final models obtained using the Rebocc algorithm. The normalized root-mean square deviation (RMSD) was evaluated at each iteration for current model m_n. For a normal distribution, the expected value of the RMSD is unity, i.e., 68% of the misfits should be less than one, and 95% less than two.

In EM induction methods, resolution directly below conductors is low and additional sensitivity tests are required. During these tests we decreased the thickness of the conductive features. At each step we checked the effect of this change on the data fit (RMSD). We ran inversion again with the modified model as a priori start model. If the RMSD was preserved, then the thickness of the conductor can still be reduced. Here we assumed that many of the conductive layers observed in Fennoscandia are often thin, like alum shales. The corresponding 2-D responses from the altered model were compared with the observed data to see the effect of the change. The same analysis was done to check the stability of other conductive features. Particularly, the feature in question was removed from the model by replacing the conductor with the background resistivity. If the conductor is not required by data, the RMSD would not changed, otherwise the RMSD of the initial model increases and inversion re-inserts the conductor back.

5.1. Crustal-scale inversion

The final 2-D inversion crustal models after sensitivity tests are shown in Fig. 10 for the seven parallel profiles. The average distance between the profiles is 50 km. There are gaps in data coverage of up to 80 km, mostly because of high topography. A homogeneous half-space initial model and an ocean a priori model were used for all inversions. The a priori model was obtained from the map of integrated conductance (*S*-map) of Fennoscandia (Korja et al., 2002). The resistivity of the initial model and other inversion parameters are presented in Table 1. Due to the expected 3-D effects and possible static shifts, higher error floors for apparent resistivity were assigned than for impedance phases. The phase of the determinant of the

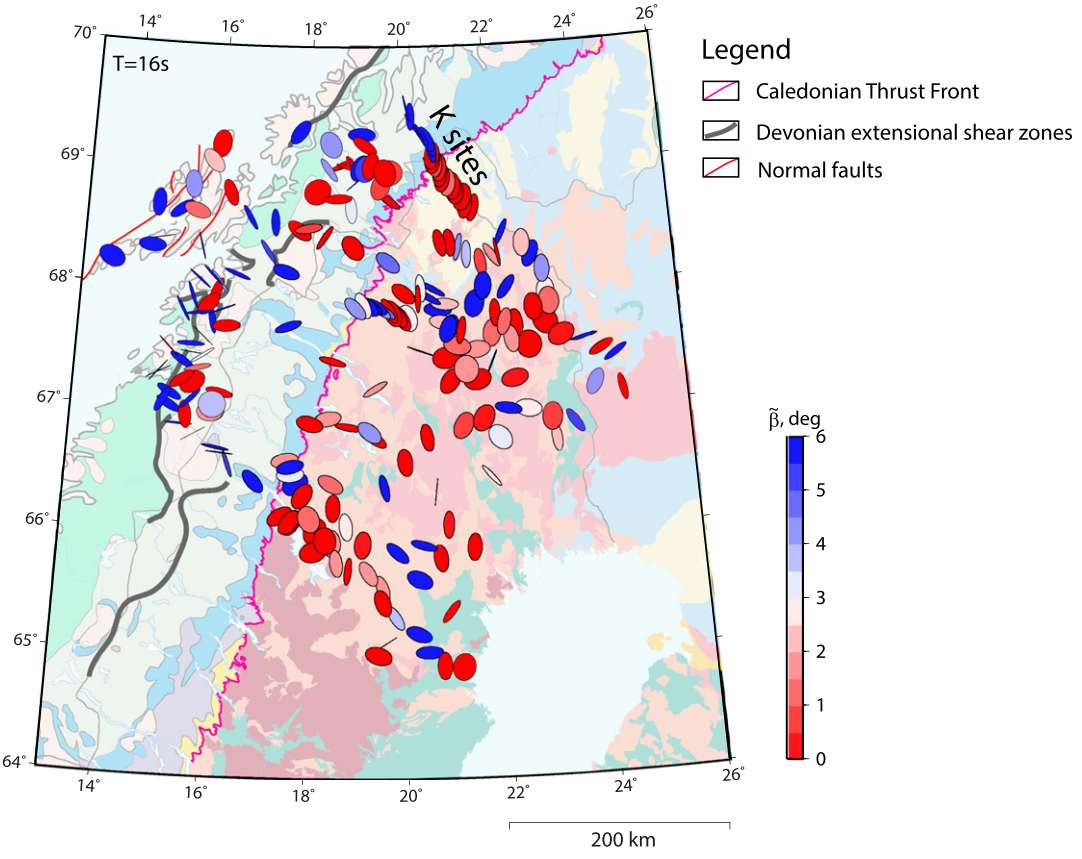

Fig. 9. The phase tensor ellipses map at a period of 16 s overlaps the geological map (Fig. 1). The colour fill is the residuals of the phase tensor skew angle $\tilde{\beta}$, Eq. (11). Red colours are considered to be quasi-2-D, blue — significant 3-D effects.

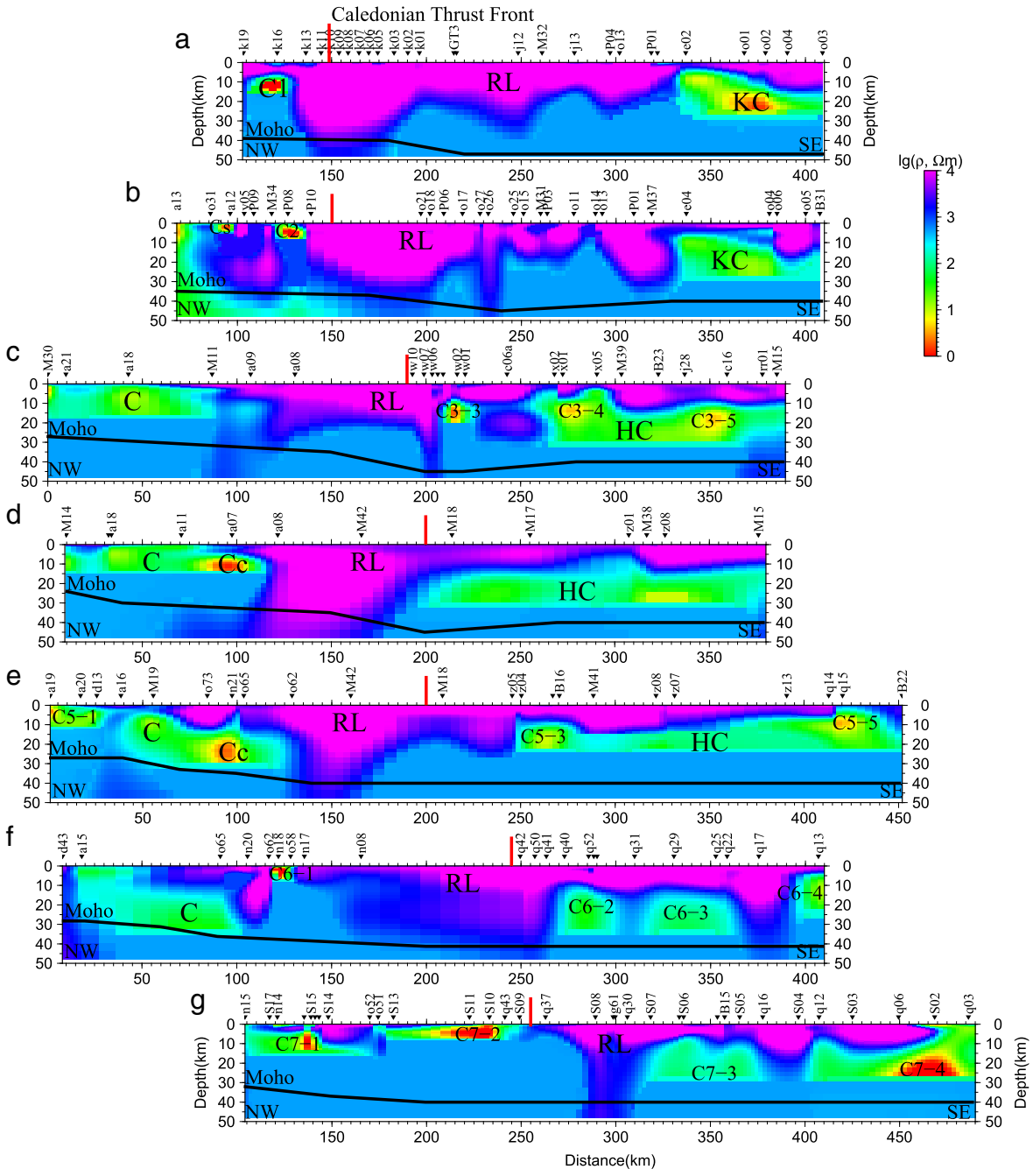

Fig. 10. Final altered models for the crustal profiles: (a)–(g) Crust 1–7. Abbreviations: RL — resistive layer, KC — Kittilä conductor, HC — horizontal crustal conductor, C — other crustal conductors. The bold black line shows the Moho depth for Fennoscandia from Grad, M., Tiira, T., Group, E.W. (2009). The red line indicates Caledonian Thrust Front.

Table 1
Crustal-scale 2-D inversion parameters. Abbreviations: N_s — number of sites; T — period range; distance — profile length; $\delta\rho_a$, %; $\delta\varphi$, ° — error floor for apparent resistivity and impedance phase in percent and degrees, respectively; ρ_{init} — resistivity of the initial model (half-space); $M_y \times M_z$ — model mesh size, M_y and M_z — number of the model parameters in y and z directions, respectively.

Name	N_s	T, s	Distance, km	$\delta\rho_a$, %; $\delta\varphi$, °	ρ_{init}, Ωm	$M_y \times M_z$	RMSD
Crust 1	27	0.003–8192	305	20; 6	10^4	234 × 97	1.2
Crust 2	28	0.003–8192	340	30; 6	10^2	225 × 85	1.7
Crust 3	23	0.003–8192	385	20; 3	10^2	225 × 85	1.7
Crust 4	13	0.003–46341	370	30; 6	10^3	205 × 93	1.3
Crust 5	22	0.003–2896	450	20; 3	10^3	243 × 80	1.0
Crust 6	22	0.003–2896	400	40; 11	10^3	221 × 80	1.1
Crust 7	33	0.003–8192	380	45; 11	10^2	275 × 85	1.1

impedance tensor is not affected by the electric effects of galvanic distortion. Thus, more weight is given to the phases.

The data misfits for crustal-scale profiles Crust 1–7 are shown in Fig. 11 for apparent resistivity (left panel) and phase (right panel) of the determinant of the impedance tensor. For most of the models the data misfit is randomly distributed, meaning that there are no systematically underfitted parts in the data. Most of the features are predicted by the data. However, there are evidences of static shift of apparent resistivity, particularly at sites: k19, P04, P01, ki14 (Crust 1), y05, o21 (Crust 2), q51 (Crust 6), q23, S08 and S04 (Crust 7). In the Crust 1 model, the eastern part is poorly fitted and deviations of the phase at long periods reach values of 6°. The same for Crust 7 profile, the poor fit of the phase is observed at most of the sites. The profile Crust 4 is characterized by sparse site spacing, the average distance between sites is 30 km. The total RMSD values of the models are shown in Table 1.

5.1.1. Resistive layer RL

An extensive crustal resistive layer (RL) of 10^4 Ωm can be observed in all inversion models. RL extends from the surface to 10 km in the east, gradually thickens to 50 km (or more) towards the west and vanishes to a few kilometres thickness in the west. The thickest part of RL is best presented in the Crust 1 profile, because of the dense site coverage (Fig. 10a, Crust 1: 130–200 km of the profile distance). On other profiles (Crust 2–6) the thickness of RL is not clear because of the larger gaps in site spacing. It is possible that RL is not a coherent structure, but smaller features, such as C7-2 in Crust 7, cannot be resolved because of the gaps. We performed tests on synthetic data to find out the relation between the site spacing and the size of the anomaly. One test shows that if the size of the conductor is less than twice of the gap between sites, the feature cannot be resolved. Another test with the model Crust 7 was undertaken. We removed three sites above upper crustal conductor C7-2

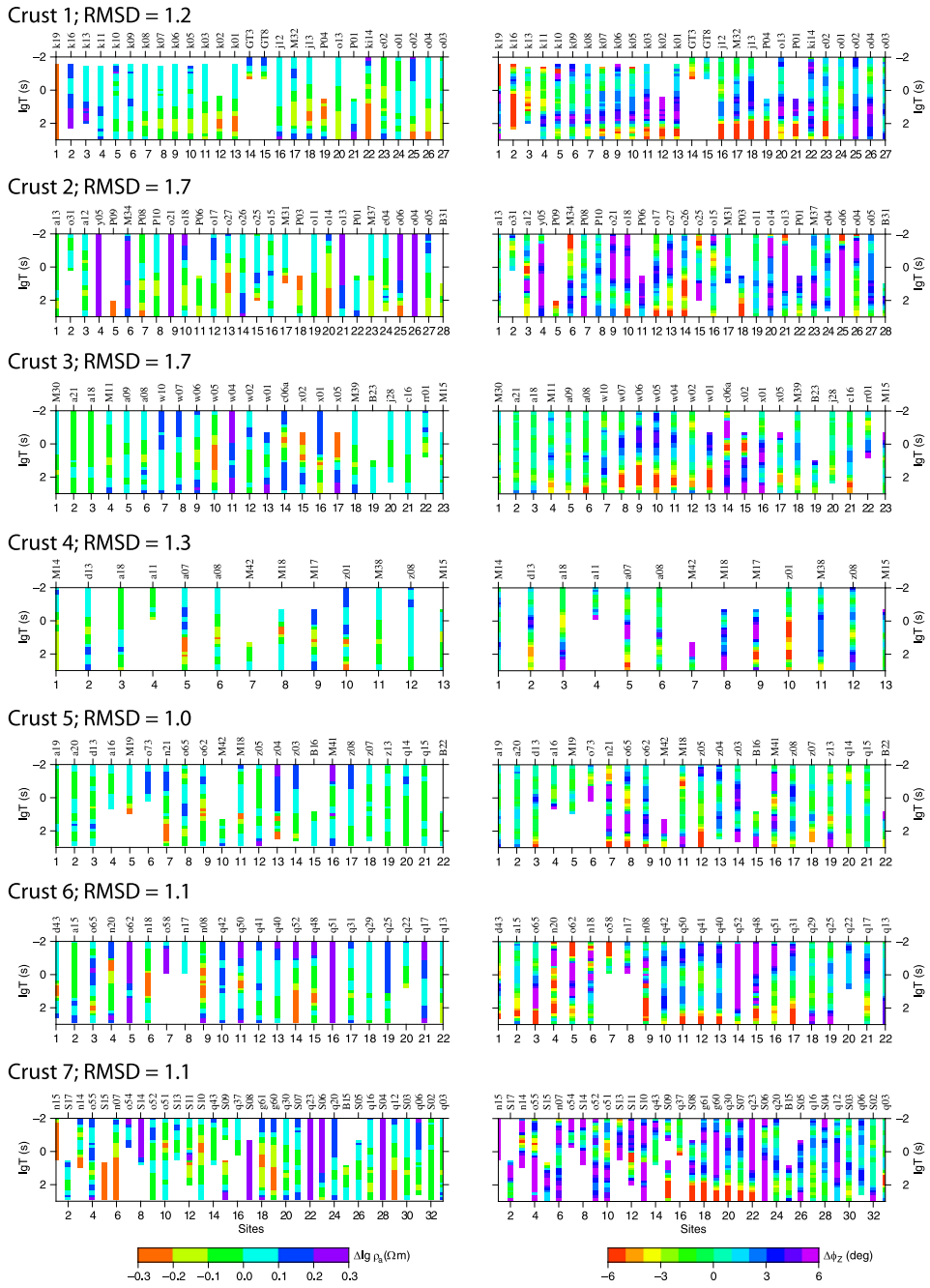

Fig. 11. Pseudo-sections of apparent resistivity misfits (left panel) and impedance phase misfits (right panel) for the determinant of the impedance tensor.

(S11, S10, q43) and ran inversion with this data set; the final test model do not represent feature C7-2. In the east, RL is a horizontal layer, extending from the surface to 10–15 km. The lower boundary of RL in the east is mostly defined by the underlying conductors and some variations in thickness of RL can be observed.

Where RL does not exist, the lower crust is generally more conductive. The conductivity changes from a few hundreds of Ωm to 10^3 Ωm. However, the conductivity of the lower crust is mostly defined by the upper and mid-crustal conductors.

5.1.2. Conductor KC

The stable conductive unit KC (Kittilä conductor) is observed at location 335–400 km of profiles Crust 1 and 2 (Fig. 10a and b, respectively). The resistivity of KC increases from 1 Ωm in its core part to 100 Ωm south-eastward, suggesting that profile Crust 2 represents the southern end of KC. The top of conductor KC has an apparent dip towards the south-east, from 5 km to 15 km, on both profiles. The resolution test showed that feature KC is strongly required by data. Removing KC from the final model leads to a change of RMSD from 1.2 to 2.6 for Crust 1. The 2-D forward responses are shown in Fig. 12 for site o01, located above KC (profile Crust 1). Black circles represent observed data, and blue circles represent responses from the model without conductor KC. The blue curves do not fit the observed data and, taking into account that inversion returned KC at first iteration, we conclude that KC is a required feature. Another test was done for the depth of the base of KC. We decreased the depth of the base of KC to 30 km, resulting in a small change in RMSD misfit, from 1.2 to 1.23. Further reduction results in a significant increase of RMSD. A comparison of the responses from the final inversion model (red) with the case of 30 km KC (green) shows that both models fit equally well (Fig. 12).

5.1.3. Conductor HC

An extensive horizontal mid-crustal conductor (HC) is observed in the central profiles (Crust 3, 4 and 5, Fig. 10c, d and e). An example of responses from the HC is site z08 located above HC (Fig. 3), the apparent resistivity and impedance phase reflect the deep conductor. The resistivity of conductor HC is around 100 Ωm with its upper boundary at a depth of 10 km. In our original models, HC extended into upper mantle. However, sensitivity tests allowed us to decrease thickness to 25–30 km without increasing the RMSD. Interestingly, we found the opposite; the reduction of HC thickness for model (Fig. 10c) improves RMSD from 1.8 for the final inversion model to 1.71 for the test model. For further reduction in depth the RMSD rises again. Regarding models Fig. 10d and e, the RMSD was preserved until depths of 30 km and 25 km were reached for (d) and (e) respectively. Thus, we conclude that at least 30 km depth extent of feature HC is required by data. Small conductive features can be identified within HC, for example on Crust 3 and Crust 5 profiles (marked as C3-3, C3-4, C3-5, C5-3 and C5-5). Feature HC is seen as a more homogeneous structure in Crust 4 profile, possibly because of sparse site spacing as the distance between sites is 40–50 km. In model Fig. 10c, the conductive spot C3-3 is a stable feature, removing it from the model increases the RMSD by 0.5. We conducted a sensitivity test on the homogeneity of feature HC. When we changed the resistivity of HC (Fig. 10c) to 200 Ωm, removing C3-4 and C3-5, the RMSD increased from 1.4 to 2.95. Then we set the background resistivity to 50 Ωm, but the RMSD still increased to 2.1. Similar features are identified in Crust

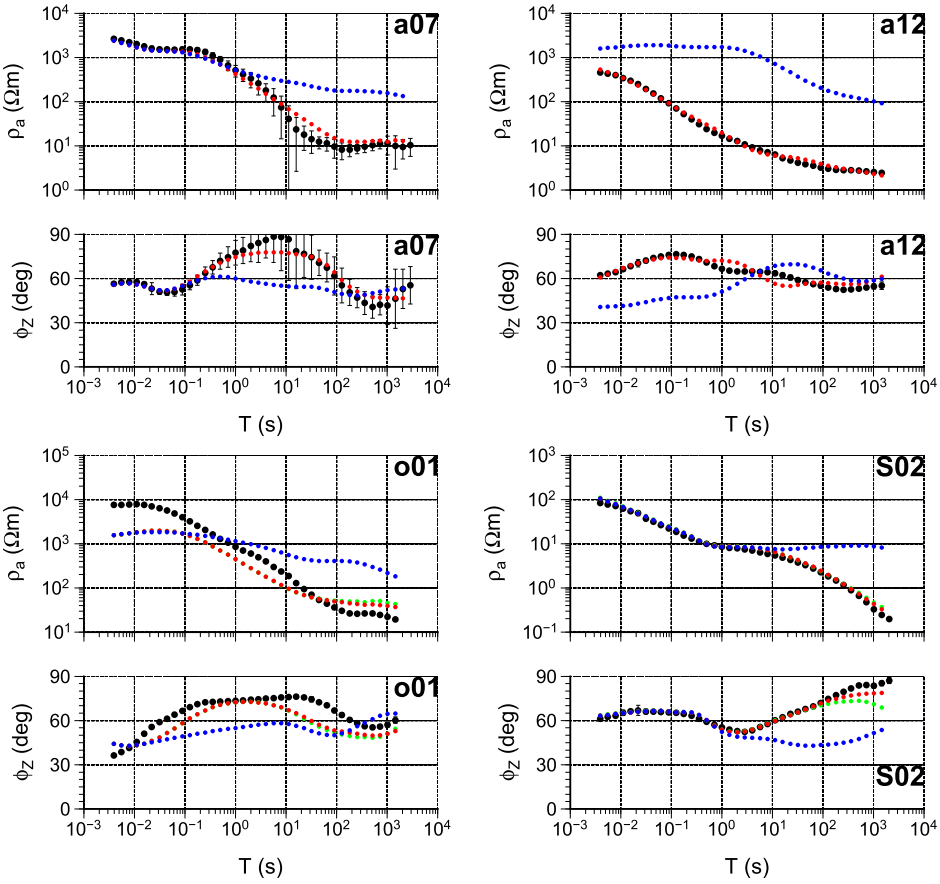

Fig. 12. Sensitivity analysis. Apparent resistivity and phase of the determinant of the impedance tensor for sites o01 (Crust 1), a12 (Crust 2), a07 (Crust 4) and S02 (Crust 7). Black circles — observed data, red circles — 2-D response from the final models (Fig. 10), blue circles — sensitivity test response for the altered model with removed conductors (for example, o01 blue circles represent the response from the model with removed KC, S02 — C7-4, a07 — Cc, a12 — Cs), green circles — sensitivity test on the depth of conductor: o01 — depth of KC is 30 km, S02 — depth of C7-4 is 30 km (see Fig. 2 for locations of the sites).

5 profile (Fig. 10e): C5-3 and C5-5. However, removing C5-3 increases RMSD from 1.1 to 1.3 and removing C5-5 increases the RMSD to 1.67. Thus, we conclude that zones of enhanced conductivity within conductor HC are required by our data.

5.1.4. Upper crustal conductors Cs, C1 and C2

Small upper crustal conductors (Cs and C2) can be observed in the western part of Crust 2 profile. The resistivity of Cs is around 10 Ωm and C2 is more conductive, around 1 Ωm. In Fig. 12, the apparent resistivity and impedance phase curves are shown for site a12 located above conductor Cs (Fig. 10b). Black and red circles show the observed and modelled responses. The blue curves represent the altered model response with removed feature Cs and do not fit the observed data, therefore we conclude that feature Cs is required by data. The sensitivity test for conductor C2 shows that it is strongly required by data. We removed feature C2 from the final model and ran the inversion again, and the RMSD increased twofold. The sensitivity tests for the depth of the conductors suggest at least 5 km for Cs and 10 km for C2, preserving the RMSD.

Conductor C1 on Crust 1 is also a robust feature. During the test, C1 was excluded from the model by replacing it with the background resistivity of 1000 Ωm. This resulted in an increase of the RMSD by 0.4. Though in final inversion model feature C1 extended to a depth of 30 km, the sensitivity tests we performed allowed us to decrease the depth of the base of the conductor to 15 km. Further reduction of the thickness of C1 leads to a significant increase in RMSD value. Therefore, we estimated the thickness of C1 to be at least 15 km.

5.1.5. Middle and lower crustal conductors C and Cc

In the west, the upper and middle crust is characterized by approx. 100 Ωm resistivity. The conductor C stretches from north to south through profiles Crust 3, 4, 5, and 6 dipping from surface to 15 km. It is possible that C extends further to the north; there is a conductive feature below site a13 (Crust 2 profile), that could be part of feature C. Sensitivity tests show that the lower boundary of C is 15 km on the northern profile and dips to 30 km southward. The distance between profiles is about 50 km, therefore the overall length of C can be estimated to be around 200 km, if we suppose it starts at Crust 2 and vanishes below Crust 6 profile.

The smaller more conductive unit Cc is located at 5 km depth on the Crust 4 profile and dips southward to 15 km below Crust 5. Together, C and Cc can represent the same conductor that outcrops in the north-west and dips south-eastward. Sensitivity tests show that anomaly Cc on both profiles is required by data; on the Crust 4 profile, removing Cc leads to increase of RMSD by 0.5 and on Crust 5 by 0.4. Examples of the apparent resistivity and impedance phase for site a07, located above Cc, are shown in Fig 12. The blue curve represents the 2-D responses from the model without conductor Cc, and the red one are the responses from the final inversion model (Fig. 10d and e). The blue curve does not fit observed data (black circles). Thus, we conclude that Cc is required by data.

5.1.6. Upper crustal conductors C5-1, C6-1, C7-1, and C7-2

There is an upper crustal conductor, labelled C5-1, at the western-most end of Crust 5 profile (Fig. 10e). This conductor is a robust feature of the data; removing C5-1 from the model increases RMSD by 2.25. A sensitivity test on the depth of C5-1 suggests value of 15 km without a change in RMSD. C5-1 can be also seen in Crust 3 and 4, below sites M30 and M14, respectively. The apparent resistivity and impedance phase for site M30 are presented in Fig. 3.

The near-surface conductor C6-1, on Crust 6, is stable and removing it from the model increases RMSD from 1.1 to 2.56. The conductor is 7–10 km in thickness and 1–5 Ωm in resistivity. A similar robust feature is seen on the Crust 7 profile — C7-1. Removing C7-1 from the final model leads to change of RMSD from 1.1 to 1.5. According to our sensitivity tests, the required minimum depth extent of conductor C7-1 is 15 km. Another strong near-surface conductor C7-2 extends from the surface to a depth of 7 km. C7-2 is a robust feature and removing it from the final model increases RMSD to 2.17 from 1.0.

5.1.7. Middle-to-lower crustal conductor C7-4

The highly conductive middle-to-lower crustal unit C7-4 is identified in the eastern part of Crust 7 profile. The top of the conductor lies at 15 km and lower boundary is not resolved. In the final inversion model, C7-4 extends to the depth of 100 km. However, sensitivity test allows us to decrease this value to 30 km, preserving RMSD. Fig. 12 shows apparent resistivity and impedance phase curves for site S02, located above conductor C7-4. Black circles represent observed data, red circles represent the responses from the final inversion model with an RMSD of 1.1, and the green circles show the 2-D responses for the model with decreased depth of C7-4 to 30 km with RMSD of 1.12. C7-4 which is required by data; removing it from the model increases RMSD to 1.53, blue circles.

5.1.8. Middle crustal conductors C6-1, C6-2, C6-4 and C7-3

In the east, mid-crust has resistivity of a few hundreds of Ωm, due to conductors C6-2, C6-3, C6-4 and C7-3 (Fig. 10f and g). The top of the conductors lies at 15 km and lower boundary is at 30–35 km. The conductors are stable features and removing them from the model increases RMSD by 0.4 in Crust 6 model and by 0.3 in Crust 7.

5.2. Lithospheric-scale inversion

The lithospheric-scale inversion is aimed at resolving the thickness of the lithosphere. Three parallel profiles Lithos 1–3 with the azimuth of N135°E and one profile Lithos 4 with the azimuth of N45°E were selected for 2-D inversion. The average distance between the parallel Lithos 1–3 profiles is 140 km and the azimuth is the same as in the case of crustal-scale inversion (Fig. 2). On the other hand, MaSca array crosses the Archaean–Proterozoic boundary (Luleå–Jokkmokk Zone in Fig. 1, Section 1) NW–SE directed. Therefore, we undertook inversion for the perpendicular profile Lithos 4.

All inversion models were obtained using Rebocc 2-D inversion code and are presented for depths of 0–400 km in Fig. 13. A polar colour scale is used from blue to red through white, and the white colour corresponding to 100 Ωm shows the interface between what we broadly term as resistive and conductive rocks, thought to be nominally the thickness of the lithosphere (see discussion later in Section 6). Similar to the crustal-scale inversions, a homogeneous half-space was used as the initial models and the ocean bathymetry included a priori in all inversions. The inversion parameters can be found in Table 2.

The final inversion models for Lithos 1–4 profiles are shown in Fig. 13. The first two profiles, (a) and (b), show generally a similar geometry for the LAB (defined here by the depth to the 100 Ωm contour). The thickness of the lithosphere is 250 km in the north-west of the profile Lithos 1 and it is gradually thinning to 200 km south-eastward. On the profile Lithos 2 the LAB is at a depth of 200 km everywhere, except the region between profile distances 270 km and 310 km. The presence of the crustal conductor significantly reduces resolution in this region (the question mark in Fig. 13b). The model from the southern profile Lithos 3 shows a deep lithosphere in the north-west (300 km), however the lithosphere thins to 150–200 km south-eastward. Note that there is a region of low resolution at a profile distance of 440 km (the question mark in Fig. 13c), therefore the thickness of the lithosphere is not well defined there. The perpendicular profile Lithos 4 crosses the profiles Lithos 1–3 at their south-eastern parts. The 2-D model from the profile Lithos 4 is consistent with the models from the parallel profiles. Particularly, the LAB is at a depth of 200 km with the small variations of ±20 km.

Pseudo-sections of the absolute misfit for apparent resistivity and impedance phase are shown in Fig. 14. Generally, data misfit is

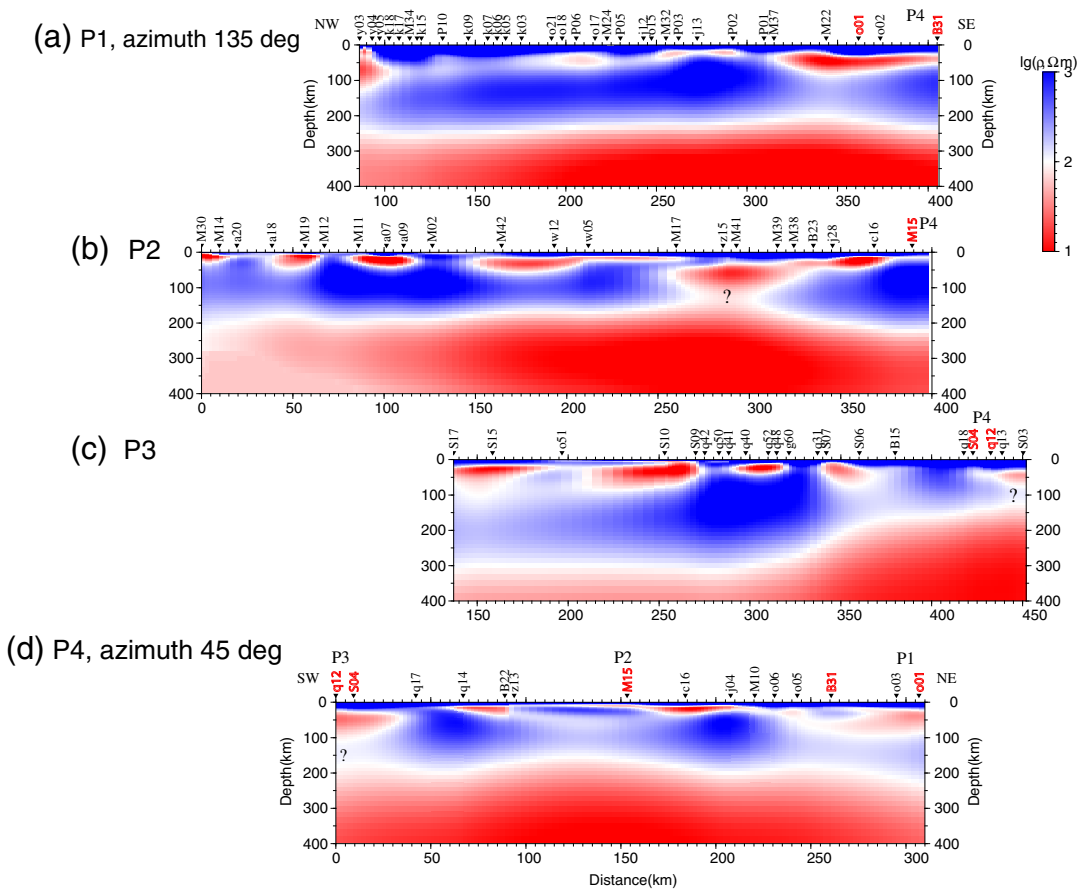

Fig. 13. Final 2-D lithospheric-scale inversion models for profiles Lithos 1–3 (a)–(c) with the azimuth of N135°E and profile Lithos 4 (d) with the azimuth of N45°E (see Fig. 2 for location). The polar colour scale is from 10 Ωm to 1000 Ωm. White colour corresponds to 100 Ωm and indicates lithosphere–asthenosphere boundary.

randomly distributed, but there are regions of systematically poor fit. For example, the north-westernmost 8 sites in Lithos 1 are fit worse for both apparent resistivity and phase. On the Lithos 2 profile, the impedance phase is fit better than apparent resistivity. The poor fit for apparent resistivity and impedance phase can be seen at sites q12 and S03 in profile Lithos 3. Static shift is observed at sites o01 and B23, and the apparent resistivity has large misfits over the entire period range.

6. Interpretation

6.1. Crustal structures

Crustal thickness increases significantly from the coast beneath the Scandinavian Mountains and further (to more than 40 km) beneath Sweden (Ebbing et al., 2012). In the north-east, the upper crust of the Precambrian basement is homogeneous and highly resistive from the surface down to 20 km (RL in Fig. 10). The resistive Precambrian basement here consists of rocks of the northern Svecofennian volcanic belt (province). In the northernmost part, the resistive rocks cross the south-western edge of the Archaean Domain and are spatially associated with Archaean gneisses (profiles Crust 1 and 2 in Fig. 2). Since the southward edge of the Archaean Domain appears to have been formed by rifting (Gaál and Gorbatschev, 1987), detached fragments of Archaean crust could possibly occur in the Svecofennian volcanic belt.

Svecofennian resistive rocks extend to the lower crust under the Caledonian Thrust Front thickening to 50 km westwards (the thickest part of RL located below the Caledonian Thrust Front). In the south the crustal resistive region can be associated with the Trans-Scandinavian granitoids, which extend to great depth (Olesen et al., 2002). The aeromagnetic data imply that the Precambrian igneous rocks of the Fennoscandian Shield can be followed below the Caledonian nappes to the tectonic windows in northern Norway (Olesen et al., 2010).

The upper crust in Norway is resistive and consists of Caledonian nappes, underlined by Precambrian basement. The basement below the Caledonides is supposed to belong to the northern Svecofennian

Table 2
Lithospheric-scale 2-D inversion parameters. Abbreviations: N_s — number of sites; T — period range; distance — profile length; $\delta\rho_a$, %; $\delta\varphi$, ° — error floor for apparent resistivity and impedance phase in percent and degrees, respectively; ρ_{init} — resistivity of the initial model (half-space); $M_y \times M_z$ — model mesh size, M_y and M_z — number of the model parameters in y and z directions, respectively.

Name	N_s	T, s	Distance, km	$\delta\rho_a$, %; $\delta\varphi$, °	ρ_{init}, Ωm	$M_y \times M_z$	RMSD
Lithos 1	32	0.003–8192	320	20; 3	10^3	200 × 103	1.8
Lithos 2	22	0.003–8192	390	20; 3	10^3	227 × 103	1.1
Lithos 3	21	0.003–8192	315	20; 3	10^3	208 × 103	2.0
Lithos 4	15	0.003–8192	310	20; 3	10^3	127 × 103	1.7

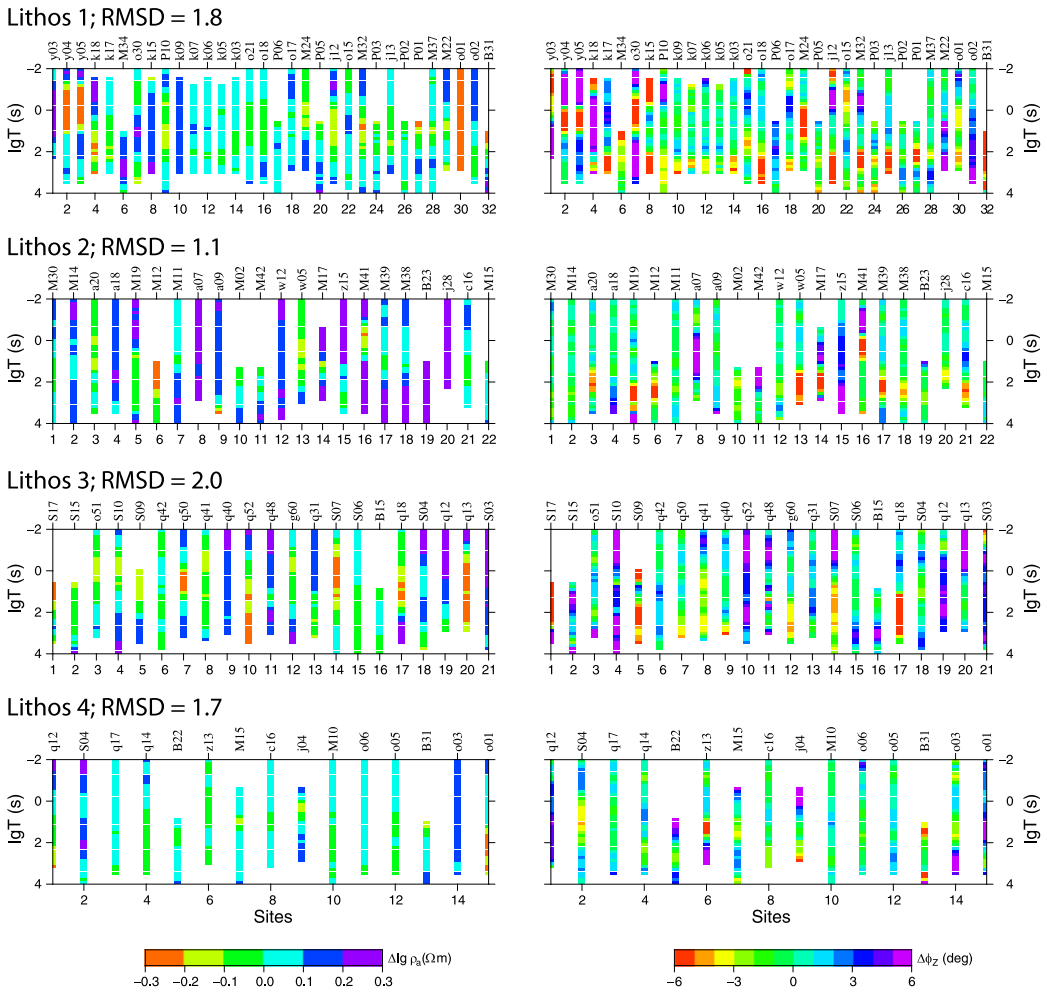

Fig. 14. Pseudo-sections of the absolute misfit for apparent resistivity (left panel) and phase (right panel) of the determinant of the impedance tensor.

volcanic belt and to consist mostly of Archaean and Palaeoproterozoic rocks, such as metagranites, granulites, gneisses, metabasalts and amphibolites, and partly of Caledonian nappes (Ebbing et al., 2012).

The middle to lower crust in northern Svecofennian province is more conductive (Fig. 10). At a crustal-scale, in particular in the Precambrian Shield areas, the only viable candidates to enhance electrical conductivity are graphite or carbon in grain-boundary films (Duba et al., 1988; Frost et al., 1989; Jödicke, 1992; Raab et al., 1998), graphite in the metamorphosed deposits of black shales (Boerner et al., 1996; Korja and Koivukoski, 1994), (Korja et al., 1996), sulphides (Jones et al., 1997; Korja et al., 1996) and iron oxides (Duba et al., 1994). Elsewhere, in Fennoscandia, similar conductors usually represent metamorphosed carbon- and sulphide-bearing sedimentary rocks, transported into deep crustal levels by tectonic processes (Hjelt et al., 2006; Korja et al., 1996; Korja et al., 2002; Korja et al., 2008). An area of enhanced conductivity, marked HC, within the conductive middle and lower crust in the northern Svecofennian province is located at the depth of 15 km and the lower boundary at 30 km. The conductor can be spatially associated with the volcanic continental Arvidsjaur–Kiruna arc (Juhlin et al., 2002), implying a tectonic model of multiple accretion of island arcs.

In the north-east, a region of the enhanced conductivity of a few thousands of Siemens is observed in the upper and mid-crust (KC in Fig. 10). The survey area is located in the western and northern parts of the Central Lapland Greenstone Belt (CLGB) that is one of the largest Proterozoic greenstone belts in the world. The CLGB consists of a Palaeoproterozoic (2.5–1.97 Ga) volcanic and sedimentary cover rocks that were deposited on Archaean (>2.5 Ga) basement. The conductor in the Kittilä district dips from the near surface (2 km) to the mid-crust (25 km) towards the north-east. The highest conductivities are related to N–S elongated graphite- and sulphide-bearing schists of the CLGB, which are visible also in the airborne electromagnetic data of the study area (Lahti et al., 2012).

The Skellefteå region is also characterized by shallow strong conductivity anomalies at the depth of 2–5 km. This was known since the early Geomagnetic Depth Sounding study of Jones (1981) (called the "Storavan" anomaly in that paper) and the subsequent MT study of Rasmussen et al. (1987). These conductive features are related to the ore bearing Skellefteå Group (1.89–1.88 Ga, (Skyttä et al., 2011)) and the overlaying Vargfors Group (1.88–1.87 Ga, (Billstrom and Weihed, 1996)), comprising turbiditic sedimentary rocks, shales, conglomerates and local intercalations of volcanic rocks (Allen et al., 1996; Årebäck et al., 2005; Weihed et al., 1992) (Fig. 1). Similar anomalies at the same depth have been observed in this region, 90 km further to the south. These anomalies have been interpreted as graphite in black shales in the contact between metasediments and metavolcanics (Hübert et al., 2013). In our Crust 7 model, the strong conductor C7-4 is observed near the Skellefteå district, but the depth of the conductor is too large to be interpreted as the Skellefteå conductor. However, the shallow conductive layer below sites S02 and q03 could represent the black shales of Vargfors group.

Recent seismological experiments from the Caledonides indicate that the preserved Caledonian allochthon in central Scandinavia is 10–12 km thick (England and Ebbing, 2012). The Caledonides are

presented as a relatively thin veneer above Precambrian basement, the thickness of which range from a few metres in the Caledonian Front in the east, gradually thickening to the depth of 5 km towards the west. In the Jämtland region, it was found in the MT study by Korja et al. (2008) that resistivity of the Caledonian allochthons varies by one order of magnitude, but they are generally resistive. The resistivity of the middle/upper allochthons varies from a few thousands to 10^5 Ωm while the lower allochthon is more conductive having resistivity from a few hundreds to a few thousands Ωm.

Extensive drilling in the Jämtland region (Andersson et al., 1985) has shown that a few metres to tens of metres of thick alum shale layers are below the Caledonian rocks and may enhance the conductivity in the uppermost crust. There are highly conductive upper crustal units in the west, below the Caledonian Thrust Front. For example, the C1, Cs1, Cs2, C2, C6-1, C7-1 and C7-2 conductors in Crust 1, 2, 6 and Crust 7 profiles, respectively. These conductors may be associated with the alum shales, the autochthonous Cambrian carbon-bearing black shales on the top of the Precambrian basement and subordinate conglomerates and sandstones, crop out at the Caledonian Front. Alum shales are known to be electrically highly conducting (Gee, 1972). It is also possible that the C1 and C2 conductors on the Crust 1 and 2 profiles represent an alum shale layer overlain by the resistive rocks of the Caledonian nappes in the north and outcropping towards the south. We conjecture that alum shales can be seen in other profiles along or near the Caledonian Front. However, the gaps in sites coverage do not allow us to resolve these small near-surface conductors.

An extensive conductive layer C + Cc stretching from north to south is located 40–120 km to the west of the Caledonian Thrust Front. The conductor dips south-eastward. The location of C and Cc coincides with the mica schists of the uppermost allochthon. These rocks of the exotic origin belong to the eastern margin of Laurentia or to a microcontinent between Laurentia and Baltica. The mica schists may contain highly conductive material, such as shales or clay rocks (Chisholm, 2011). The Caledonian nappes trusted in a NE direction and the uppermost allochthon mica schists can represent the first 5 km of C on Crust 3 and 4. Another possible explanation is saline fluids (Becken and Ritter, 2012) infiltrated in the Sagfjorden shear zone (Fig. 1). The Sagfjorden shear zone may have governed the location of the large-scale, Mesozoic, normal fault zones that bound the sides of the Lofoten and Utrøst Ridges (Olesen et al., 2002). It should be noted that EM methods are extremely sensitive to the presence of a minor amount of partially interconnected conducting phases distributed in large volumes, such as fluids or carbon.

The basement below the Caledonides is thought to belong to the northern Svecofennian volcanic belt, where enhanced conductivity was explained by the presence of the metamorphosed carbon- and sulphide-bearing sedimentary rocks. Therefore, we assume that the same causes of the enhanced conductivity may occur in the western part of the northern Svecofennian volcanic belt. A similar middle to lower crustal conductor has been identified in the Jämtland–Trøndelag region (Korja et al., 2008) further to the south. The enhancement of the average crustal conductivity there was associated with Caledonian related processes or later opening of the Atlantic Ocean, which also might have affected the lower crust. We also suggest that the mid-crustal conductor identified in our 2-D models, might be a northern extension of the Jämtland–Trøndelag conductor.

In the westernmost margin of the Fennoscandian Shield, under the Lofoten, conductive unit can be observed at the depth of about 5 km (C5-1 in Crust 5). There is no clear evidence of the causes of the enhanced conductivity here. The Lofoten consists of the Archaean and Proterozoic rocks of ancient Baltica, exposed to the surface during Devonian extension. Thus, it is unlikely that the rocks of the uppermost allochthon extend below the Lofoten. Possible explanation of the enhanced conductivity below the Lofoten is the presence of the saline fluids in complicated fault system within the Lofoten.

6.2. Electric LAB

The results of the 2-D inversion from four MT profiles in northwestern Fennoscandia suggest that the thickest lithosphere is in the Palaeoproterozoic Svecofennian province (Fig. 13d). This is supported by the previous studies of Korja (2007) and Jones (1999). From our results, the thickness of the Palaeoproterozoic lithosphere reaches 300 km depth and the Archaean lithosphere is 200 km to 250 km. Jones (1983) evaluated the thickness of the lithosphere in Kiruna as 173 ± 15 km and in Nattavaara as 211 + 27/−23 km (Fig. 1). From our measurements, the thickness in Kiruna (near site w05, Lithos 2 profile Fig. 13b) is around 170 km and in Nattavaara (near sites j28 in Lithos 2 Fig. 13b) is 200 km. The thickness of the lithosphere from Korja (2007) is 250 km. Korja (2007) concluded that the thickest lithosphere is in the Palaeoproterozioc Svecofennian Domain, which is in agreement with our models (the lithosphere is thickening to 300 km towards the south). On the other hand, the thinning of the lithosphere towards the Atlantic Ocean suggested by Korja (2007) is not supported by our results. Note, that the resolution of the new array is far better than the previous compilations, where the distance between sites was 50 km (BEAR array).

7. Conclusions

We have conducted magnetotelluric measurement within the "Magnetotelluric in the Scandes" (MaSca) project, during the summers of 2011–2013. All together data at 220 broad-band and 59 long period sites were measured. The array crosses the major tectonic structures within the Precambrian and younger Caledonian rocks. Two important borders are crossed: the Archaean–Proterozoic boundary and the Caledonian Thrust Front.

- The overall data quality is good. The apparent resistivity varies from 0.1 Ωm to 10^5 Ωm reflecting areas of the high conductivity and resistivity. The phases are consistent and show the region of the low conductivity between 0.1 and 100 s. There are some long period MT sounding curves reaching a period of 10^5 s.
- Two methods were used for strike and dimensionality analyses: the phase tensor and Q-function. Both analyses revealed generally 2-D behaviour of the data with 3-D effects at some sites and period bands. In the north-east, in the Precambrian part, a NS strike is identified for periods 0–100 s. For longer periods, the average strike of N45°E can be identified from the rose diagram of Q-function. In the Caledonides, the strike is more complicated.
- The induction vectors have been used for strike analysis. For shorter periods, the induction vectors point in different directions, reflecting the 3-D near-surface structures. For longer periods, their behaviour is more consistent between each other as well as with the Q-function rose diagrams. The vectors are reflecting the conductive ocean in the west and the influence of the strong Skellefteå conductor in the south.
- The comparison of the Q-function and phase tensor analyses showed their consistency. The greatest advantage of the Q-function analyses is that it gives the quantitative estimate of the deviation of the data from the 2-D assumption.
- The phase tensors were also compared with the induction arrows. High levels of agreement were observed for all data.
- The crustal-scale 2-D inversions have been done for seven profiles and lithospheric-scale for four profiles. The averaged strike direction of N45°E is used.
- The inversion models show the resistive Precambrian basement and the conductive middle to lower crust in the northern Svecofennian volcanic province. The enhanced conductance can be explained by the presence of the graphite-bearing rocks and sulphides. In the north the upper crustal conductor is seen as the southern end of the Kittilä greenstone belt. The enhanced conductivity there is related to graphite- and sulphide-bearing schists, which are visible also in the airborne electromagnetic data of the study area.

• In the Caledonides, the presence of the highly conductive alum shales is observed along the Caledonian Thrust Front. The regional highly conductive upper crustal units are shown in the 2-D inversion models. The extensive conductive features are closely located along the uppermost allochthon mica schists, which can also contain the conductive material.

• The thickest lithosphere is in the Palaeoproterozioc Svecofennian Domain, not in the Archaean. The thickness of the lithosphere is 200 km in the north and 300 km in the south-west of the MaSca array.

• An extension of the MaSca measurements is planned along the Blue Road seismic profile (Section 1). In addition results from the SCANLIPS 2 seismic profile in northern Norway will be available in the coming years and they will facilitate modelling of the processes that shaped the topography of the Scandinavian Mountains (England and Ebbing, 2012).

Acknowledgements

We would like to thank Lars Dynesius for help in preparing the field work, Colin Hogg and Maxim Smirnov Jr. for help during the field work. Financial support was provided by the Academy of Finland (272912 and 136345).

References

Agustsson, K., 1986. A magnetotelluric pilot study in the Scandes. Geol. Fören. Stockh. Förh. 108, 258–261.
Allen, R., Weihed, P., Svenson, S., 1996. Setting of Zn–Cu–Au–Ag massive sulfide deposits in the evolution and facies architecture of a 1.9 Ga marine volcanic arc, Skellefte district, Sweden. Econ. Geol. Bull. Soc. Econ. Geol. 91, 1022–1053.
Andersen, T.B., 1998. Extensional tectonics in the Caledonides of southern Norway, an overview. Tectonophysics 285, 333–351.
Andersson, A., Dahlman, B., Gee, D.G., Snäll, S., 1985. The Scandinavian Alum Shales. Sveriges Geologiska Undersökning (SGU), Serie Ca, NR 56 pp. 1–49.
Årebäck, H., Barrett, T., Abrahamsson, S., Fagerstrom, P., 2005. The Palaeoproterozoic Kristineberg VMS deposit, Skellefte district, northern Sweden, part I. Geology. Mineral. Deposita 40, 351–367.
Bahr, K., 1991. Geological noise in magnetotelluric data: a classification of distortion types. Phys. Earth Planet. Inter. 66, 24–38.
Becken, M., Ritter, O., 2012. Magnetotelluric studies at the San Andreas Fault Zone: implications for the role of fluids. Surv. Geophys. 33, 65–105.
Berdichevsky, M., Pokhotelov, D., 1997. Violation of the dispersion relations in a three-dimensional magnetotelluric model. Izv. Phys. Solid Earth 33, 603–608.
Billstrom, K., Weihed, P., 1996. Age and provenance of host rocks and ores in the Paleoproterozoic Skellefte District, northern Sweden. Econ. Geol. 91, 1054–1072.
Boerner, D.E., Kurtz, R.D., Craven, J.A., 1996. Electrical conductivity and Paleo-Proterozoic foredeeps. J. Geophys. Res. 101, 13775–13791.
Booker, J., 2012. The magnetotelluric phase tensor: a critical review. Surv. Geophys. 35, 7–40.
Brasse, H., Kreutzmann, A., Cerv, V., Ernst, T., Jankowski, J., Jozwiak, W., Neska, A., Pedersen,, L.B.r., Smirnov, M., Schwarz, G., Sokolova, E., Varentsov, I.M., Hoffmann, N., Palshin, N., Korja, T., 2006. Probing electrical conductivity of the Trans-European Suture Zone. EOS Trans. Am. Geophys. Union 87, 281.
Caldwell, T.G., Bibby, H.M., Brown, C., 2004. The magnetotelluric phase tensor. Geophys. J. Int. 158, 457–469.
Cherevatova, M., Smirnov, M., Korja, T., Kaikkonen, P., Pedersen, L., Hübert, J., Kamm, J., Kalscheuer, T., 2014. Crustal structure beneath southern Norway imaged by magnetotellurics. Tectonophysics 628, 55–70.
Chisholm, H., 2011. "Petrology". Encyclopedia Britannica, 11 edition Cambridge University Press.
Constable, S.C., Parker, R.L., Constable, C.G., 1987. Occam's inversion: a practical algorithm for generating smooth models from electromagnetic sounding data. Geophysics 52, 289–300.
Duba, A., Huengest, E., Nover, G., Will, G., Jödicke, H., 1988. Impedance of black shale from Mönsterland I borehole: an anomalously good conductor? Geophys. J. 94, 413–419.
Duba, A., Heikamp, S., Meurer, W., Mover, G., Will, G., 1994. Evidence from borehole samples for the role of accessory minerals in lower-crustal conductivity. Nature 367, 59–61.
Ebbing, J., England, R., Korja, T., Lauritsen, T., Olesen, O., Stratford, W., Weidle, C., 2012. Structure of the Scandes lithosphere from surface to depth. Tectonophysics 536–537, 1–24.
England, R.W., Ebbing, J., 2012. Crustal structure of central Norway and Sweden from integrated modelling of teleseismic receiver functions and the gravity anomaly. Geophys. J. Int. 191, 1–11.
Frost, B.R., Fyfe, W.S., Tazaki, K., Chan, T., 1989. Grain-boundary graphite in rocks and implications for high electrical conductivity in the lower crust. Nature 340, 134–136.
Gaál, G., Gorbatschev, R., 1987. An outline of the Precambrian evolution of the Baltic shield. Precambrian Res. 35, 15–52.
Gee, D.G., 1972. The Regional Geological Context of the Tåsjö Uranium Project, Caledonian Front, Central Sweden. Sveriges Geologiska Undersökning (SGU) Serie C, Central Sweden, pp. 1–36.
Gee, D.G., Fossen, H., Henriksen, N., Higgins, A.K., 2008. From the early Paleozoic platforms of Baltica and Laurentia to the Caledonide Orogen of Scandinavia and Greenland. Episodes 31, 44–51.
Gorbatschev, R., Bogdanova, S., 1993. Frontiers in the Baltic Shield. Precambrian Res. 64, 3–21.
Grad, M., Tiira, T., Group, E.W., 2009. The Moho depth map of the European Plate. Geophys. J. Int. 176, 279–292.
Groom, R.W., Bailey, R.C., 1989. Decomposition of magnetotelluric impedance tensors in the presence of local three-dimensional galvanic distortion. J. Geophys. Res. 94, 1913–1925.
Guggisberg, B., Kaminski, W., Prodehl, C., 1991. Crustal structure of the Fennoscandian Shield: a traveltime interpretation of the long-range FENNOLORA seismic refraction profile. Tectonophysics 195, 105–137.
Hjelt, S.E., Korja, T., Kozlovskaya, E., Lahti, I., Yliniemi, J., SVEKALAPKO Seismic Tomography W. G., BEAR, W.G., 2006. Electrical conductivity and seismic velocity structures of the lithosphere beneath the Fennoscandian Shield. Geol. Soc. Lond. Mem. 32, 541–559.
Hübert, J., Juanatey, M.d.l.A.G., Malehmir, A., Tryggvason, A., Pedersen, L.B., 2013. The upper crustal 3-D resistivity structure of the Kristineberg area, Skellefte district, northern Sweden revealed by magnetotelluric data. Geophys. J. Int. 192, 500–513.
Jödicke, H., 1992. Water and graphite in the Earth's crust—an approach to interpretation of conductivity models. Surv. Geophys. 13, 381–407.
Jones, A.G., 1981. Geomagnetic induction studies in Scandinavia. J. Geophys. 50, 23–36.
Jones, A.G., 1983. The electrical structure of the lithosphere and asthenosphere beneath the Fennoscandian Shield. J. Geomagn. Geoelectr. 35, 811–827.
Jones, A.G., 1999. Imaging the continental upper mantle using electromagnetic methods. Lithos 48, 57–80.
Jones, A.G., 2012. Distortion decomposition of the magnetotelluric impedance tensors from a one-dimensional anisotropic Earth. Geophys. J. Int. 189, 268–284.
Jones, A.G., 2013. Imaging and observing the electrical Moho. Tectonophysics 609, 423–436.
Jones, A.G., Spratt, J., 2002. A simple method for deriving the uniform field MT responses in auroral zones. Earth, Planets and Space 54, 443–450.
Jones, A.G., Katsube, T.J., Schwann, P., 1997. The longest conductivity anomaly in the world explained: sulphides in fold Hinges causing very high electrical anisotropy. J. Geomagn. Geoelectr. 49, 1619–1629.
Juhlin, C., Elming, S., Mellqvist, C., Öhlander, B., Weihed, P., Wikström, A., 2002. Crustal reflectivity near the Archaean–Proterozoic boundary in northern Sweden and implications for the tectonic evolution of the area. Geophys. J. Int. 150, 180–197.
Koistinen, T., Stephens, M.B., Bogatchev, V., Nordgulen, O., Wennerström, M., Korhonen, J., 2001. Geological map of the Fennoscandian Shield, scale 1:2 000 000. Espoo: Trondheim: Uppsala: Moscow: Geological Survey of Finland: Geological Survey of Sweden: Geological Survey of Norway: Ministry of Natural Resources of Russia.
Korja, T., 1993. Electrical conductivity distribution of the lithosphere in the central Fennoscandian Shield. Precambrian Res. 64, 85–108.
Korja, T., 2007. How is the European lithosphere imaged by magnetotellurics? Surv. Geophys. 28, 239–272.
Korja, T., Koivukoski, K., 1994. Crustal conductors along the SVEKA Profile in the Fennoscandian (Baltic) Shield, Finland. Geophys. J. Int. 116, 173–197.
Korja, T., Hjelt, S.E., Kaikkonen, P., Koivukoski, K., Rasmussen, T.M., Roberts, R.G., 1989. The geoelectric model of the POLAR Profile, Northern Finland. Tectonophysics 162, 113–133.
Korja, T., Tuisku, P., Pernu, T., Karhu, J., 1996. Lapland Granulite Belt — implications for properties and evolution of deep continental crust. Terra Nova 8, 48–58.
Korja, T., Engels, M., Zhamaletdinov, A., Kovtun, A., Palshin, N., Tokarev, A., Smirnov, M., Asming, V., Vanyan, L., Vardaniants, I., BEAR, W.G., 2002. Crustal conductivity in Fennoscandia — a compilation of a database on crustal conductance in the Fennoscandian Shield. Earth Planets Space 54, 535–558.
Korja, T., Smirnov, M., Pedersen, L., Gharibi, M., 2008. Structure of the Central Scandinavian Caledonides and the underlying Precambrian basement, new constraints from magnetotellurics. Geophys. J. Int. 175, 55–69.
Lahti, I., Korja, T., Kaikkonen, P., Vaittinen, K., BEAR, W.G., 2005. Decomposition analysis of the BEAR magnetotelluric data: implications for the upper mantle conductivity in the Fennoscandian Shield. Geophys. J. Int. 163, 900–914.
Lahti, I., Korja, T., Smirnov, M., Vaittinen, K., Sandgren, E., Niiranen, T., Nykänen, V., 2012. 3-D imaging of the Central Lapland Greenstone Belt using magnetotelluric and seismic data 14, 2652 p.
Lund, C.E., 1979. The fine structure of the lower lithosphere underneath the Blue Road profile in northern Scandinavia. Tectonophysics 56, 111–122.
Lund, C.E., Heikkinen, P., 1987. Reflection measurements along the EGT POLAR-profile, northern Baltic Shield. Geophys. J. R. Astron. Soc. 89, 361–364.
Olesen, O., Lundin, E., Nordgulen, O., Osmundsen, P.T., Skilbrei, J.R., Smethurst, M.A., Solli, A., Bugge, T., Fichler, C., 2002. Bridging the gap between onshore and offshore geology in Nordland, northern Norway. Nor. J. Geol. 82, 243–262.
Olesen, O., Brönner, M., Ebbing, J., Gellein, J., Gernigon, L., Koziel, J., Lauritsen, T., Myklebust, R., Sand, M., Solheim, D., Usov, S., 2010. New aeromagnetic and gravity compilations from Norway and adjacent areas — methods and applications. Pet. Geol. Conf. Ser. 7, 559–586.
Pedersen, L.B., Engels, M., 2005. Routine 2D inversion of magnetotelluric data using the determinant of the impedance tensor. Geophysics 70, G33–G41.
Raab, S., Hoth, P., Huenges, E., Müller, H.J., 1998. Role of sulfur and carbon in the electrical conductivity of the middle crust. J. Geophys. Res. 103, 9681–9689.

Ramberg, I.B., Bryhni, I., Nøttvedt, A., Rangnes, K. (Eds.), 2008. The Making of a Land — Geology of Norway. Norwegian Geological Association, Trondheim.
Rasmussen, T.M., 1988. Magnetotellurics in southwestern Sweden: evidence for electrical anisotropy in the lower crust? J. Geophys. Res. Solid Earth 93, 7897–7907.
Rasmussen, T.M., Roberts, R.G., Pedersen, L.B., 1987. Magnetotellurics along the Fennoscandian long range profile. Geophys. J. R. Astron. Soc. 89, 799–820.
Roberts, D., 2003. The Scandinavian Caledonides: event chronology, palaeogeographic settings and likely modern analogues. Tectonophysics 365, 283–299.
Rykkelid, E., Andresen, A., 1994. Late Caledonian extension in the Ofoten area, northern Norway. Tectonophysics 231, 157–169.
Siripunvaraporn, W., Egbert, G., 2000. An efficient data-subspace inversion method for 2D magnetotelluric data. Geophysics 65, 791–803.
Skyttä, P., Hermansson, T., Andersson, J., Weihed, P., 2011. New zircon data supporting models of short-lived igneous activity at 1.89 Ga in the western Skellefte District, central Fennoscandian Shield. Solid Earth 3, 355–383.
Smirnov, M.Y., 2003. Magnetotelluric data processing with a robust statistical procedure having a high breakdown point. Geophys. J. Int. 152, 1–7.
Smirnov, M.Y., Egbert, G.D., 2012. Robust principal component analysis of electromagnetic arrays with missing data. Geophys. J. Int. 190, 1423–1438.
Smirnov, M.Y., Pedersen, L.B., 2009. Magnetotelluric measurements across the Sorgenfrei–Tornquist Zone in southern Sweden and Denmark. Geophys. J. Int. 176, 443–456.
Smirnov, M., Korja, T., Dynesius, L., Pedersen, L., Laukkanen, L., 2008. Broadband magnetotelluric instruments for near-surface and lithospheric studies of electrical conductivity: a Fennoscandian pool of magnetotelluric instruments. Geophysica 44, 15–27.
Varentsov, I.M., Engels, M., Korja, T., Smirnov, M., the BEAR Working Group, 2002. A generalized geoelectric model of Fennoscandia: a challenging database for long-periods 3D modelling studies within the baltic electromagnetic array research (BEAR) progect. Izvestya. Phys. Solid Earth 38 (10), 855–896.
Weidelt, P., Kaikkonen, P., 1994. Local 1-D interpretation of magnetotelluric B-polarization impedances. Geophys. J. Int. 117, 733–748.
Weihed, P., Bergman, J., Bergström, U., 1992. Metallogeny and tectonic evolution of the Early Proterozoic Skellefte district, northern Sweden. Precambrian ResearchPrecambrian Metallogeny Related to Plate Tectonics 58 pp. 143–167.
Zhang, P., Roberts, R.G., Pedersen, L.B., 1987. Magnetotelluric strike rules. Geophysics 52, 267–278.